TFIIIC dynamically binds Alu elements to control gene expression through chromatin looping

Roberto Ferrari[*1§], Lara Isabel de Llobet Cucalon[*1], Chiara Di Vona[1], Enrique Vidal[1], Antonios Lioutas[1], Francois Le Dilly[1], Javier Quilez Oliete[1], Giorgio Dieci[2], Martin Teichmann[3], Susana de la Luna[1,4,5] and Miguel Beato[1,4,§]

Affiliations

1- Gene Regulation Stem Cells and Cancer Program, Center for Genomic Regulation (CRG), Barcelona Institute of Science and Technology (BIST), Barcelona, Spain.

2- Department of Chemistry, Life Sciences and Environmental Sustainability, University of Parma, Parco Area delle Scienze 23/A, Parma, Italy

3- Université de Bordeaux INSERM U1212 - CNRS UMR 5320 146, rue Léo Saignat 33076 Bordeaux France

4- Universitat Pompeu Fabra (UPF), Barcelona, Spain

5.- Institució Catalana de Recerca i Estudis Avançats (ICREA), Barcelona, Spain

* These authors contributed equally to this work.

§ Co-corresponding authors: roberto.ferrari@crg.eu, miguel.beato@crg.eu

Highlights

- Serum starvation enhances TFIIIC binding to Alu Elements (AEs) near cell cycle genes
- Binding of TFIIIC increases H3K18 acetylation over the bound AE
- TFIIIC-mediated looping to distal genes favors their reactivation upon serum addition
- Long-range TFIIIC interactions tune cell cycle genes expression through nuclear repositioning

Graphical abstract

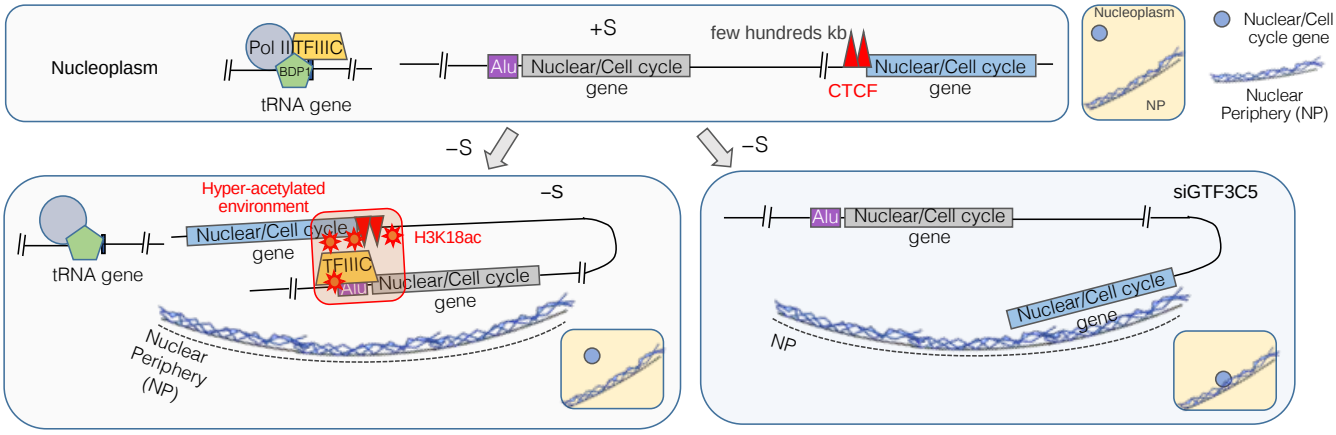

Summary

Folding of the mammalian genome is governed by architectural proteins, such as CTCF. TFIIIC, a RNA polymerase III transcription factor, has been identified as an insulator but its role in genome topology is totally unknown. Here, we show that TFIIIC establishes long-range genomic interactions that affect gene expression. Upon serum starvation (SS), TFIIIC occupancy increases at Alu elements (AEs) near promoters of cell cycle-related genes. Bound AEs become H3K18 hyper-acetylated and fold to contact distal pre-loaded CTCF sites near other cell cycle genes. The promoters of these genes also become hyper-acetylated ensuring their basal transcription during SS and their increased expression during serum re-exposure. Ablation of TFIIIC or deletion of the TFIIIC-bound AE that loops to the G2/M cycling F (*CCNF*) locus affects its expression and nuclear positioning. These results illustrate a novel function of human TFIIIC in changing 3D genome topology through the epigenetic state of AEs.

Keywords

TFIIIC, Alu elements, transposons, H3K18ac, histone acetylation, breast cancer, CTCF, Hi-C, 3D genome structure, Pol II, Pol III, cell cycle, *CCNF*, *UHRF1*.

Introduction

Transcriptional regulation is crucial for the organization and coordination of cellular functions during rapid changes in environmental conditions (Lee and Young, 2013). In the last decade, it has become clear that 3D folding of the eukaryotic genome at the level of chromosome compartments, topologically associating domains (TADs) and long-distance contacts between regulatory elements, is established during cell differentiation by the combined action of lineage specific transcription factors (TFs) in cooperation with architectural proteins, such as CCCTC-binding factor (CTCF) and Cohesins (Stadhouders et al., 2018).

In higher eukaryotes, the expansion of several families of transposable elements (TE) has provided new regulatory sequences enabling coordinated control of gene expression (Chuong et al., 2017). Short Interspersed Elements (SINEs), in particular Alu elements (AEs), represent a fraction of TE that have evolved proto-enhancers function in the human genome (Su et al., 2014). A recent analysis has provided evidence for a strong positive correlation between AEs density and the overall level of chromatin interactions (Gu et al., 2016). AEs are transcribed by RNA polymerase III (Pol III), a nutrient-sensing machinery that also transcribes tRNA and other small non-coding RNA genes (Dieci et al., 2007). Pol III recruitment depends on prior binding of transcription factor TFIIIC to intragenic sequence-specific promoters encompassing so-called A and B boxes, followed by recruitment of TFIIIB (Dieci et al., 2007). Besides its known function in Pol III transcription, TFIIIC has also been shown to possess several other activities (Donze, 2012). Like CTCF, TFIIIC can act as an insulator and participates in 3D genome organization from yeast to mammals (Pascali and Teichmann, 2013; Van Bortle and Corces, 2012). TFIIIC is

also capable of binding so-called Extra TFIIIC sites (ETC) (Moqtaderi et al., 2010), which carry a non-canonical B-box and are devoid of the remaining Pol III machinery. TFIIIC binding to these sites is central to the ETC's peripheral localization mechanism in budding yeast (Hiraga et al., 2012). In mouse, TFIIIC binding to SINE controls the relocation of the activity-dependent neuronal genes *Fos* and *Gadd45a* to transcription factories (Crepaldi et al., 2013). In *Drosophila*, TFIIIC and other insulator proteins redistribute within the genome upon heat shock to rewire DNA looping within TADs favoring proper gene expression in response to environmental cues (Li et al., 2015).

Serum deprivation (or serum starvation, from here on abbreviated as SS) is widely used to synchronize cultured cells (Pirkmajer and Chibalin, 2011), although it has been shown to trigger a plethora of distinct responses (Pirkmajer and Chibalin, 2011). The response to SS *in vivo* allows tumorigenic cells to activate survival pathways in the face of reduced nutrient availability (Anastasiou, 2017). In primary human fibroblasts, genome organization is considerably altered upon SS, with chromosome territories quickly re-localizing within interphase nuclei as cells enter a reversible SS-induced quiescence (Mehta et al., 2010). However, very little is known about the molecular mechanisms involved in SS induced changes of the 3D genome structure. To explore this question, we decided to investigate the role of TFIIIC and CTCF in human cells under SS using ChIP-seq, along with RNA-seq, epigenetic profiling, microscopy and in situ Hi-C analysis. We uncovered a reversible mechanism by which upon SS TFIIIC (but not CTCF) augmented its binding at AE close to annotated transcription start sites (TSS) of Pol II-transcribed genes enriched in cell cycle functions. Docking of TFIIIC enhances histone 3 lysine 18 (H3K18)

acetylation (H3K18ac) of AEs, which correlates with a slight decrease in both Pol II loading and expression of the AE and its nearby gene. Simultaneously, the TFIIIC-bound AEs establish long-range intra-TADs interactions with pre-bound CTCF sites within promoters of cell cycle relevant genes, which become H3K18 acetylated, maintains their basal levels of transcription, and relocate them to a nuclear environment that may facilitate activation upon serum re-exposure.

Results

TFIIIC occupancy at AEs increases during SS

To explore how human insulators behave following SS, we employed ChIP-seq to map the genome occupancy of CTCF and TFIIIC in growing T47D breast cancer cells (full media with fetal bovine serum [FBS] added) and after 16 h of SS (Figure S1A). We chose these conditions because they have been used to synchronize the cells for hormone regulation studies and are well tolerated with no indication of apoptosis or other forms of cell death (Le Dily et al., 2014) (Figures S1A and S1B). Small changes in the number, the distribution, or the intensity of the CTCF peaks were observed upon SS (Figure 1A, top panel and Figure 1C left panel). In marked contrast, SS induced a large number of TFIIIC binding sites, passing from 388 to 3362 (Figure 1A, bottom panel). Around 36% of the total TFIIIC peaks (134) were located over tRNA genes in normal growth conditions, whereas this percentage decreased to only 1% (33) upon SS (Figure 1B). In contrast, whilst only 30% (140) of the total TFIIIC peaks were located over AEs in normal growth conditions, this value increased to 89% (3096) after SS, mostly representing the gain of TFIIIC peaks in this condition (Figure 1B). Finally, 28% of the TFIIIC sites (107) were located over other sequences (5S RNA, 7SLRNA and other sub-pericentromeric repeats such as ALR/Alpha) in the presence of serum, and their number did not change upon SS. Word cloud analysis of major repetitive elements (RE) bound by TFIIIC clearly confirmed the switch, showing AEs as highly enriched after SS, in particular the AluSx family (Figure S1C), a relatively young Alu lineage (~30 million years old), which still exhibits a small mobilization activity (Bennett et al., 2008). We found that the majority of the AEs bound by TFIIIC are *bona fide* functional AEs as

defined by having intact A- and B-boxes. When we looked for B-box consensus of ETC sites (Moqtaderi et al., 2010), we found only 459 occupied sites, corresponding to 14% of the SINEs bound by TFIIIC under SS (Figure S1D).

The comparison of the genome occupancy for CTCF and TFIIIC in the two experimental conditions, indicated that the degree of overlap between the peaks was low for TFIIIC and very high for CTCF (Pearson's correlation coefficients: r=0.61 for TFIIIC and r=0.89 for CTCF) (Figure 1C, Tables S1 and S2). A browser image of several examples is shown in Figure 1D. The shift of TFIIIC genome occupancy was also evident when its total significant counts at tRNA genes or AEs were plotted before and after SS (Figures S1E and S1F). Loss of TFIIIC binding to tRNA genes upon SS was also evident at the chromosomal level with chromosomes 1 and 6, which contain the largest tRNA clusters, losing their TFIIIC enrichment upon SS (Figures S1G and S1H). Moreover, increased occupancy of AEs in -S was reflected in TFIIIC enrichment in gene-rich chromosomes such as chromosomes 16, 17 and 19 (Figure S1H), which were previously reported to display high AEs density (Bolzer et al., 2005).

AEs bound by TFIIIC are near Pol II promoters and devoid of any other Pol III factor

We then asked whether the AEs occupied by TFIIIC following SS exhibited any peculiar genomic distribution. We plotted the distance of each TFIIIC peak to the closest Pol II TSS using Genomic Regions Enrichment of Annotations Tool (GREAT) (McLean et al., 2010), and found that the fraction of peaks mapping in close proximity (within 5 kb) of annotated TSSs increased upon SS, and the fraction of distantly located (>50 kb) sites was greatly diminished (Figure 1E). We also

explored whether other components of the Pol III machinery were enriched at the TFIIIC bound AE, using antibodies to B-Double Prime (BDP1), a component of the essential TFIIIB complex, and to the Pol III holoenzyme subunit F or RPC39. We found that BDP1 and RPC39 were enriched at tRNA genes independently of the growth conditions, but we did not detect significant occupancy of these factors at AEs sites bound by TFIIIC upon SS (Figures 1D, S1I and S1J). As a control, we show that TFIIIC was bound to the *RNA7SL2* gene on chromosome 14 in a serum-independent manner, while Pol III and TFIIIB binding decreased upon SS (Figure S1K), in agreement with the finding that *in vitro* transcription of Pol III units longer than a tRNA gene (≥75 bp) is TFIIIC-dependent (Ferrari et al., 2004).

SS-dependent increased TFIIIC occupancy at AEs is rapidly reversible and occurs in tumor and non-tumor cells

Increased number of TFIIIC peaks were also observed in other normal and cancer cell lines subjected to SS, such as MCF10A cells, an immortalized normal breast epithelial cell line, the glioblastoma cell line T98G and the normal lung fibroblasts IMR90 (Figure 2A and S2A). Genome-wide Pearson's correlation for the significant TFIIIC counts in the four cell lines analyzed indicated a larger degree of similarity between the breast samples compared to lung and glioblastoma, and between non-tumor cells compared to cancer cells (Figure 2B).

Similarly to T47D, a large fraction of TFIIIC peaks was associated with AEs following SS in MCF10A cells (Figure S2B), while other components of the Pol III machinery did not appear to be recruited at TFIIIC-bound AEs upon SS (Figure S2C), further supporting the uniqueness of

TFIIIC binding to AEs nearby Pol II-transcribed genes. As for the breast cell lines, also T98G and IMR90 showed increased genome-wide occupancy of TFIIIC after SS at AEs (Figures S2D and S2E). All together these data point to a conserved mechanism of SS-induced TFIIIC enrichment at a subset of AEs in the proximity of Pol II promoters independently of the tissue origin of the cell line.

Finally, we asked whether TFIIIC increased binding at AEs in T47D cells could be reverted by serum re-addition to the media. TFIIIC occupancy at regions bound in the absence of serum and enriched in AEs was almost vanished within 30 min of serum addition (Figure 2C). This behavior was also observed in T98G cells (Figure 2D). These results show that TFIIIC recruitment in response to growth conditions is a reversible process; furthermore, they also rule out a cell-cycle direct role in dictating TFIIIC binding to AEs, as 30 min after serum re-addition are not sufficient for the cells analyzed to re-enter cell cycle.

TFIIIC-associated Pol II promoters (TAPs) display increased AEs H3K18ac but minor changes in transcription and Pol II occupancy

We next investigate the properties of these TFIIIC-associated Pol II promoters (TAPs). Using a 10 kb window around the TSS we identified 1,490 TAPs (Figure 3A and Table S3), which were all bound by TFIIIC upon SS and enriched for GO terms related to cell cycle, in particular, to G1/S phase transition and mitosis (Figure S3A). TAPs were significantly enriched in binding motifs related to T-box transcription factor (TBX3), SP2 and the cell cycle-related transcription factor E2F3 (Figure S3B). Notably, the TFIIIC enrichment at AEs close at TAPs was not simply

reflecting a higher AE density, since after sorting all Pol II promoters by the presence/absence of TFIIIC we found that non-TAPs exhibited higher AEs density than TAPs (Figure S3C and Table S4**)**. We therefore conclude that the enrichment is due to increased recruitment of TFIIIC at TAPs.

Given that TFIIIC possesses histone acetyl-transferase (HAT) activity (Kundu et al., 1999) and interacts with p300/CREB-binding protein (CBP) (Mertens and Roeder, 2008), we explored whether TAPs exhibit increased H3K18ac, a marker of p300/CBP function *in vivo* (Ferrari et al., 2008; Jin et al., 2011). A comparison of H3K18ac levels at TAPs before and after SS revealed that binding of TFIIIC after SS markedly correlates with increased H3K18ac (Figure 3B; see also Figure 3C for *MCM2* as an example).

MCM2 has an AE located close to its TSS, which is transcribed from the opposite DNA strand with respect to the MCM2 transcriptional direction (Figure 3C). Upon SS, TF3C recruitment to the AE is observed in all cell lines analyzed, which is accompanied by increased H3K18ac restricted to the AE bound by TF3C (Figure 3C). Globally, the H3K18ac signal at all TAPs upon SS clearly overlapped with the center of the associated AE (Figure 3D). In contrast, neither TFIIIC binding nor H3K18ac showed enrichment upon SS on tRNA genes (Figure 3E). Around 78% of all AEs bound by TFIIIC (2,417 out of 3,096) were found to be significantly acetylated at H3K18 (Figure 3F), and a similar percentage was found when the analysis was restricted to TAPs upon SS (1027 out of 1490) (Figure 3G). Thus, H3K18 acetylation of TAPs is increased only at their associated AEs.

To determine the expression level of the TAP genes, we performed poly-A mRNA-seq before and after SS, and found that TAPs exhibited higher levels of RNA expression than a random group of equivalent size in both +S and –S conditions, but showed a not drastic, but significant reduction in transcription upon SS (Figure 3H). This reduction could be due to a not drastic, albeit significant, reduction of Pol II occupancy at TAPs upon SS (Figure S3D and S3E). The expression level of the AEs was also slightly reduced upon SS (Figure S3F), but we could not detect changes of Pol III or BDP1 at the same loci (Figures 1D and Figure S1I).

SS leads to extensive changes in mRNA expression, many of them dependent on TFIIIC

To determine the global role of TFIIIC on gene expression, we assessed gene expression changes in cells depleted of TFIIIC. We used siRNAs targeting *GTF3C5* (the gene encoding the fifth largest subunit of TFIIIC), since it has been shown that its yeast homolog stabilizes the interaction of TFIIIC with the B box (Jourdain et al., 2003). Around 3,000 genes were differentially expressed (> 1.5-fold; p-value < 0.05) when the +S and –S (non-transfected) conditions were compared in T47D, with a similar number of up-regulated (1571) and down-regulated (1438) genes (Figures 4A and S4A and Table S5). The up-regulated genes in the +S condition showed enrichment for GO terms linked to protein trafficking, translation and cell cycle (Figure S4B), in agreement with cells actively proliferating; the up-regulated genes in the -S condition, were enriched for terms related to developmental process, cell adhesion and responses to growth factor stimulus (Figure S4C).

Depletion of the GTF3C5 subunit of TFIIIC by almost 80%, both at the protein and the mRNA levels (Figure 4D, and STAR Methods), led to dysregulation of 1756 transcripts upon SS (Figure 4B). More than half of the differentially expressed transcripts were down-regulated both in comparison to –S (non-transfected) cells or to siCTRL cells (Figures 4B and S4E). Much fewer changes were observed comparing siCTRL and –S conditions (Figure S4F). Using "binding and expression target analysis" (BETA) (Wang et al., 2013), we detected statistical significant TFIIIC binding only with genes whose levels were down-regulated upon TFIIIC depletion compared to siCTRL (Figures S4G and S4H). For further analysis, we focused on the genes up-regulated (252 genes) or down-regulated (613 genes) by TFIIIC depletion during SS that did not exhibit significant changes in the siCTRL cells upon SS (Figure 4C and Table S6). These two sets of genes represent those genes that are, directly or indirectly, repressed or activated by TFIIIC in response to SS, and we named them TRGs and TAGs, respectively.

TRGs showed GO enrichment for terms such as cell projection, cilium organization, microtubule-based movement and axoneme-assembly (Figure S4I). GO analysis of TAGs showed enrichment for cell-cycle regulated activity (Figure S4J), in agreement with a recent report in glioblastoma cells (Buchel et al., 2017). Examples of cell cycle-regulated genes belonging to TAGs are the *MCM7* and the helicase lymphoid specific (*HELLS)* genes (Figure S4K). The nature of TAGs is reflected in the significant drop in the number of cells in the S- and G2/M-phases in siGTF3C5 cells, compared to siCTRL cells or SS cells (Figure S4L); in contrast, tRNA expression did not respond to GTF3C5 silencing neither in normal growth conditions nor

upon SS (Figure S4M). All together the results suggest a TFIIIC function in Pol II transcription independent of tRNA gene expression.

Finally, to explore whether TFIIIC depletion impairs histone acetylation of AEs, we measured H3K18ac enrichment at two AEs that are bound by TFIIIC upon SS. One of the AEs lies in close proximity (~1 kb) of the down-regulated gene *HELLS*; the other AE is located at a larger distance (~120 kb) from the TSS of the down-regulated ubiquitin-like protein containing PHD and RING finger domains-1 (*UHRF1)* gene. Both AEs acquired H3K18ac upon SS, and the acetylation levels were strongly reduced upon TFIIIC depletion compared to cells expressing siCTRL (Figure 4D). Taken together these results suggest that TFIIIC-dependent H3K18 acetylation of AEs could be implicated in regulating cell cycle-regulated genes upon serum deprivation.

TFIIIC binding to AEs promotes a rapid recovery of cell cycle genes expression from SS

The results so far led us to hypothesize that TFIIIC could work in maintaining the mRNA steady state levels of its target genes upon SS in order to enable a quick response to serum. To test this hypothesis, we performed mRNA-seq in SS cells expressing either siRNA against GTF3C5 or siCTRL RNA at different time intervals after serum exposure. GTF3C5 depleted levels were maintained during the time course (Figure S4N). The analysis of TAGs showed that control cells rapidly responded to serum addition by increasing their expression as soon as 3 h post-addition, while TFIIIC depleted cells did not (Figure 4E). These data further support a positive role of TFIIIC in the serum-induced expression recovery of a group of cell cycle-related genes.

We explored whether TFIIIC binding to the promoter regions of the of the genes responding to GTF3C5 knockdown is directly responsible of their regulation. We therefore computed the overlap between TAPs (TF3C-associated genes) and TAGs (TF3C-activated genes) and found that the overlap between the two sets of genes (TAPs and TAGs) was only 13% (Figure 4F). However, although the overlap was small, it showed enrichment for cell cycle-related GO terms (Figure S4P). Based on these results, and given the known role of TFIIIC as genome organizer (Van Bortle and Corces, 2012), we speculate that the regulation of genes affected by TFIIIC depletion might not only involve direct action on TAPs but could also be mediated by long-range chromatin interactions with other distant genes also involved in cell cycle control.

TFIIIC-mediated long-range interactions participate in maintaining gene expression levels during SS

To test this hypothesis, we performed *in nucleo* Hi-C (Le Dily and Beato, 2018) in T47D cells grown in the presence of absence of serum both in normal cells as well as in cells depleted of TFIIIC. When we plotted the log2 of the ratio between the “observed and expected” (O/E) interactions of TFIIIC binding sites with all the genes affected upon SS versus the ones unaffected, we found that TFIIIC sites interact more frequently with genes whose expression was affected by SS (Figure 5A).

As CTCF is enriched at promoter regions (Ruiz-Velasco et al., 2017), and it has been shown to interact with TFIIIC (Galli et al., 2013), it could facilitate the TFIIIC long-range interactions. To explore this possibility, we first plotted CTCF and Pol II occupancy at all human TSSs in T47D

and found that the CTCF binding pattern very much resembles that of Pol II. Moreover, both factors were enriched on promoter regions of TAPs (Figure 5B and Table S7). To explore how CTCF and TFIIIC interact in our experimental conditions, we performed co-immunoprecipitation experiments with a CTCF antibody in extracts from T47D cells before and after SS and probed the immunoprecipitates in western blots with a TFIIIC antibody against the GTF3C2 component (the same used in ChIP). We found that SS is accompanied by an increase of TFIIIIC interaction with CTCF-containing complexes (Figure 5C), which was not due to changes in total TFIIIC protein levels (Figure S5). Remarkably, the increased interaction between the two insulators upon SS was also reflected in the Hi-C data in form of a significant higher level of intra-TAD contacts involving the two factors (Figure 5D).

For a high-resolution analysis of these interactions we focused on two cell cycle genes, *UHRF1* and the G2/mitotic-specific cyclin-F (*CCNF*), which showed long-range interactions involving a distal TFIIIC-bound AE (Figures 6A and 6B). The Hi-C data showed that SS induced the interaction of an AE bound by TFIIIC near the promoter of the cell cycle regulated gene *FEM1A*, with the *UHRF1* gene located almost 150 kb downstream (Figure 6A, Hi-C data top and medium), while it disrupted the interaction of the same AE with a group of genes (*PLIN4/PLIN5*) located ~200 kb upstream (Figure 6A, Hi-C data top and medium). The expression of the *PLIN4/5* genes was down-regulated in the absence of serum, but unaffected by siGTF3C5, while *UHRF1* expression further responded to siGTF3C5 (Figure 6A, genome browser tracks bottom). In the case of *CCNF*, its TSS was also engaged in an interaction with an AE bound by TFIIIC located ~300 kb upstream and near the promoter of *ECI1* whose expression is cell cycle regulated

(Santos et al., 2015) (Figure 6B, Hi-C data top and medium). Using the Hi-C data, we generated a virtual 4C plot of the *CCNF* locus using the AE bound by TFIIIC as the viewpoint, which shows that the TFIIIC-bound AE increases its interaction with the downstream *CCNF* gene (Figure 6C), which is surrounded by multiple CTCF binding sites (Figure S6A). *CCNF* expression was slightly affected in the absence of serum, but it did respond to the absence of GTF3C5 (Figure 6B, genome browser tracks bottom).

Given these clear examples of chromatin looping involving AE-containing regions bound by TFIIIC, we asked how many gene promoters behave similarly. We calculated a normalized interaction score for all the AEs bound by TFIIIC during SS and all human gene promoters (see Methods) and found that more than 100 AEs were capable of significant interactions with genes whose expression was affected by the depletion of TFIIIC. Ultimately, together with the 82 genes directly bound by TFIIIC within 10 kb of their TSS (Figure 4F), we found a total of 193 genes whose expression could be affected by either local or long-range (>250 kb) interactions with a TFIIIC-bound AE (Figure 6D and Table S8). Thus, we predict that if these genes were co-regulated by TFIIIC during SS, they should be also commonly regulated between normal and serum-deprived condition. To address this question, we represented the expression level of the 193 genes from Figure 6D as a heatmap, comparing +S, siCTRL and siGTF3C5 versus SS cells. As expected, the vast majority (almost 70%) of these genes corresponded to genes down-regulated by the absence of serum, which further lowered their expression in the absence of GTF3C5 (Figure 6E). These results suggest that TFIIIC would be require to sustain basal transcription levels of a subset of cell cycle-related genes. Notably, the CTCF occupancy in the

promoters of these genes calculated as the number of binding events in a window of 10 kb around their TSS was significantly higher compared to a random set of promoters of the same size (Figure 6F).

Our results thus suggest that by analyzing SS, we uncovered that AE-bonded TFIIIC reshapes the genomic topology by promoting DNA looping between the AEs and the regulated promoters to ensure a steady state level of expression levels of a subset of cell cycle-regulated genes. It is possible that TFIIIC fulfills this role by increasing H3K18ac at AEs, and thereby the interaction with the target genes would position them in an acetylated “transcription-favorable” environment. It is also possible that the interaction might promote the spreading of the acetylated mark at distal regions. If this is the case, H3K18ac should also increase at the promoters of distant interacting genes upon SS. Indeed, depletion of serum caused a drastic change in the overall profile of H3K18ac at promoter regions (Figure S6B). Whereas in normal growth conditions H3K18ac is narrowly restricted to a region very close to the TSS, H3K18ac seemed more evenly distributed along a broader region of the promoter both up- and down-stream of the TSS in SS (Figure S6B and S6C). Remarkably, when the fraction of TFIIIC-bound promoters (both directly or via long-range interactions) was evaluated, we found that almost 70% of them had a strong increase in the histone mark upon SS (Figure S6D). All together these data causally link TFIIIC action to changes in genome topology and epigenetic marks to co-opt the regulation of a large set of relevant cell cycle-associated genes.

TFIIIC as activator and insulator

As observed for the *UHFR1* locus (Figure 6A), we also found that TFIIIC has the ability to bind AEs and to trigger a decrease of *cis*-contacts with surrounding genes, as it is apparent at the phosphoserine transferase 1 (*PSAT1*) and the heparan sulfate proteoglycan 2 *(HSPG2*) / zinc finger and BTB domain containing 40 *(ZBTB40*) loci, which exhibited a dramatic decrease of the corrected contact score up- and downstream of the AEs bound by TFIIIC upon SS (Figure S6E-S6G). This behavior could be explained by the already known TFIIIC's insulator properties (Van Bortle and Corces, 2012).

To explore the role of TFIIIC on the formation of the intra-TADs loops during SS, we analyzed the Hi-C interactions of TFIIIC-occupied sites with genes affected by TFIIIC depletion. We found that, in agreement with the BETA analysis (Figure S4G), TFIIIC binding is significantly enriched in TADs containing TAGs than in those containing TRGs (Figure 7A). We reasoned that if TFIIIC is necessary to maintain the interactions induced by SS, its depletion should decrease the total frequency of interactions. Indeed, TFIIIC depletion significantly decreased the overall intra-TAD contacts compared to the siCTRL treatment (Figure 7B). In agreement with this finding, we observed increased Hi-C normalized contact counts upon TFIIIC depletion at the *PLIN4/5* locus, resembling the situation observed in the presence of serum (Figure 7C). This was also evident in the virtual 4C of the Hi-C data (Figure S7A). Thus, the interaction that connected the AE with the *PLIN4/5* locus in the presence of serum and that disappeared in response to SS, reappeared in the TFIIIC depleted cells in SS (Figures 7C and S7A, black arrow). In contrast, the overall area

of interactions between the TFIIIC-bound AE and the *UHRF1* gene was decreased upon TFIIIC depletion (Figures 7C and S7A, red arrow).

Next, we asked whether TFIIIC binding to AEs is required for co-regulating the 193 genes identified in Figure 6D (affected by TFIIIC depletion and showing short- or long-range contacts). Based on our model, depletion of TFIIIC would lead to a reduction in the total number of interactions of the promoters of these genes with the corresponding TFIIIC-bound AE. Indeed, the interaction score for the siGTF3C5 Hi-C data was significantly decreased compared to the siCTRL (Figure 7D). Altogether, these results confirm that TFIIIC is necessary to increase the frequency of the interactions of the AE with the associated promoters in order to co-regulate a set of genes involved in cell cycle control.

As mentioned above, our data supports a role for TFIIIC in orchestrating the chromatin re-organization events that lead to the basal transcription of a subset of genes in SS. To show that the AEs are needed for this role of TFIIIC, we used CRISPR-Cas9 technology (Wang et al., 2016) to delete the AE-bound by TFIIIC between the *PLIN4/5* and *UHRF1* loci (Figure 6A; see also Figure S7B for the schematic description of the procedure and Star Methods for details). This AE contacts the *UHRF1* locus upon SS (Figure 6A), and depletion of TFIIIC causes a dramatic decrease in its expression during SS (Figures 6A, genome browser bottom). Unfortunately, from the CRISPR/Cas9-based genetic modification of T47D cells we did not obtain clones with the two alleles modified and therefore, we choose one heterozygous clone for further analysis (Figure S7C). Remarkably, deletion of the AE in just one allele caused almost 50% decrease in the expression of *UHRF1* upon SS, compared to the parental cell line (Figure 7E).

This result agrees with that from TFIIIC depletion in SS (Figure 4C) and with the Hi-C data (Figures 6A and Figure 7C), and support the requirement of the AE to maintain steady-state levels of *UHRF1* transcripts during conditions of stress. It is worth noting that the effect of the AE deletion could be even more dramatic if a homozygous clone could have been obtained.

TFIIIC and the nuclear location of cell cycle genes

Given the ability of TFIIIC to relocate genomic regions to the nuclear periphery (NP) (Hiraga et al., 2012) and that recruitment to the NP can alter gene expression by itself (Finlan et al., 2008), we wondered whether TFIIIC-regulated cell cycle genes could possibly be affected in their spatial positioning within the nucleus by this factor. We used fluorescent *in situ* hybridization (FISH) to examine the nuclear location of the *CCNF* locus and found that that SS triggers the relocation of the *CCNF* gene from the nuclear center to a more sub-peripheral shell (Figure 7F; quantification of the radial position of the *CCNF* probe from the NP is reported in Figure S7D). Notably, the *CCNF* locus was positioned even more peripherally in siGTF3C5 expressing cells than in cells expressing siCTRL (Figure 7F). Indeed, a significant decrease in the distance between the *CCNF* probe and the NP was observed upon ablation of TFIIIC (Figure 7G), in agreement with the degree of transcriptional repression observed upon GTF3C5 depletion (Figure 4C), and with the observation that peripherally-located genes tend to be less expressed (Finlan et al., 2008).

Discussion

The cellular stress response allows the organism to cope with a variety of molecular changes in the environment, including change of temperature, exposure to toxins, mechanical damage and lack of nutrients (Poljsak and Milisav, 2012). To maintain homeostasis, cells need to rapidly mount a transcriptional program that ensures survival during the stress situation and recovery once the stress finishes. However, thus far very little is known about the contribution of DNA topology and genome architectural proteins (such as CTCF, Cohesins and TFIIIC) to cellular stress response in mammalians. We report here that the cellular response to SS involves genome reorganization mediated by the Pol III transcription factor TFIIIC (Figure 7H), with TFIIIC chromatin recruitment decreasing at tRNA genes and increased binding to a set of AEs in the vicinity of Pol II promoters of genes involved in cell cycle regulation. The AE-bound TFIIIC participates in forming long-distance intra-TAD loops with the promoters of a broad range of cell cycle-regulated genes via interaction with bound CTCF, and expression of these genes depends on TFIIIC (Figure 7H). We therefore propose that the long-distance interactions mediated by TFIIIC contribute to the transcriptional regulation of the target genes maintaining basal transcription of cell cycle-regulated genes and enabling their reactivation upon serum exposure.

These findings uncover a role of TFIIIC in altering genome topology that differ from previous studies reporting the hard-wiring of promoter-enhancers chromatin loops in transcriptional response to stress (Vihervaara et al., 2017). Our model favors a more dynamic and reversible network that responds to the absence of growth factors by establishing transient new

connections between promoter-regulatory regions that maintain steady state expression levels of crucial cell cycle regulators during the SS phase (Figure 7H). The proposed model relies on TFIIIC collaborating with CTCF to establish signal regulated enhancer-promoter interactions, as described in other contexts (Weintraub et al., 2017). The model is also supported by other findings. For instance, TFIIIC subunits were identified among several factors that associate with regulatory regions (enhancers and promoters) by means of histone modification ChIP followed by mass spectrometry (MS) (Engelen et al., 2015). In addition, the TFIIIC largest subunits are known to interact with the E1A binding protein p300/CBP, an established marker of enhancers (Mertens and Roeder, 2008); this which could be linked to our observation that AEs bound by TFIIIC become hyper-acetylated in H3K18, a marker of p300/CBP activity *in vivo* (Ferrari et al., 2008; Jin et al., 2011). Curiously, we find that the TFIIIC-dependent hyper-acetylation TAPs is limited to the AEs bound by TFIIIC, and it does associate with neither increased transcription nor with higher Pol II loading of the nearby gene promoter. Although we have not identified the HAT responsible, several candidates can be envisaged, including TFIIIC, p300/CBP or the retinoblastoma protein pRB, which by interacting with the transcription factor E2F bound to the TAPs that could restrict the acetylation of H3K18 to the AEs only (Ferrari et al., 2014). Given that the long-distance CTCF bound promoters of cell cycle genes become also hyper-acetylated upon looping to the TFIIIC-bound AE, it is therefore possible that this hyper-acetylated environment may participate in genomic relocation within the nucleus to maintain basal levels of transcription in SS, and favoring the reactivation of the genes upon serum exposure. The model is in agreement with the previously reported coupling of p300-mediated acetylation and redirection of

Fos and *Gadd45a* genes to transcription factories during neuronal depolarization (Crepaldi et al., 2013), and with the results of a recent study supporting a role of chromatin state and RE enrichment in guiding chromosomal positioning within mammalian nuclei (van de Werken et al., 2017).

Characteristics of the AE bound by TFIIIC

TFIIIC recognizes A- and B-boxes as typical internal promoter elements for Pol III transcriptional units (Dieci et al., 2007), as well as with single B-boxes scattered along the genome (ETC sites) (Moqtaderi et al., 2010). AEs also contain A- and B-boxes, so they could serve as the landing platform for TFIIIC. However, as only a subset of AEs is bound by TFIIIC, additional characteristics of the bound AEs are required to explain TFIIIC selective binding. One possibility is that the AEs recognized by TFIIIC are particularly accessible in chromatin, which may be the case since the adjacent promoters are of cell cycle-regulated genes that are highly transcribed in the presence of serum. Alternatively, it is possible that the particular subset of TFIIIC-bound AEs exhibits binding sites for others TFs that may interact with TFIIIC. On this regard, our RIME (Rapid Immunoprecipitation Mass spectrometry of Endogenous proteins) data show that two of the major TFIIIC interactors are the chromodomain helicase DNA binding protein 4 (CHD4) and activity dependent neuroprotector homeobox (ADNP) (Table S9 and STAR Methods). These two proteins together with heterochromatin protein 1 (HP1) form a complex called ChAHP involved in chromatin-mediated gene regulation (Ostapcuk et al., 2018); in addition, and like TFIIIC, ADNP is enriched in active enhancers and promoters (Ji et al., 2015). Indeed, we found that ADNP is

highly enriched over AEs (Figure S7E); in particular, we detected enrichment of ADNP over the 3,096 AEs-bound by TFIIIC upon SS, the 1,490 AEs of TAPs and the 193 promoters involved in long-distance looping (Figure S7F). Thus, ADNP may participate, with TFIIIC, in DNA looping mediated via AEs. Very interestingly, we also found that mouse ADNP chromatin occupancy is mostly (95%) associated with RE (Figure S7G); almost 50% of the bound RE are B2 elements (Figure S7H), which are Alu-like elements is rodents (Kramerov et al., 1979). As all the ADNP occupancy public data have been generated in cell cultured in the presence of serum, it is possible that the ChAHP complex is constitutively bound to AEs and might facilitate the landing of TFIIIC upon SS.

TFIIIC and long-distance loops

One of our most intriguing observation is that of the set of 613 TAG genes with reduced expression in cells depleted of TFIIIC, only 82 overlapped with TAPs (Figure 4F). This indicated the existence of mechanisms other than proximity to explain TFIIIC dependency. Of course, the effect could be indirect or mediated by other TFIIIC associated factors. However, we provide evidence that part of the TAG subset (32%) is regulated by virtue of long-distance interactions of TFIIIC-bound AEs with distantly located TFIIIC-dependent genes enriched with preloaded CTCF. Our data support the requirement of both TFIIIC (siGTF3C5) and the AE (genetic ablation of the AE distal to *UHRF1*) for this effect. However, to what extent CTCF is needed for this effect remains to be proven.

In addition, there could be other mechanisms of DNA looping, that could not be caught by regular Hi-C experiments, might explain the altered expression of the remaining group of genes and that could not be caught by regular Hi-C experiments. It is also possible that the hyper-acetylated regions created by TFIIIC constitute a special environment that could allow phase separation, where DNA proximity could maintain basal levels of transcription (van de Werken et al., 2017). Of note, TFIIIC contains several subunits with large unstructured domains (Male et al., 2015), and disorder protein regions have been shown to promote phase separation (Boeynaems et al., 2018).

TFIIIC and nuclear location of cell cycle genes

The finding that SS induces an alteration of the TFIIIC occupancy in human cells begs the question of what is the functional role of TFIIIC binding to AEs. TFIIIC-dependent reactivation is likely due to a proper positioning of the target genes within the nucleus, as TFIIIC ablation triggers a strong peripheral recruitment of the cell cycle gene *CCNF*, which coincides with its full repression. In our view, the presence of TFIIIC, bound to the hyper-acetylated AEs, represents a barrier for the otherwise strong peripheral recruitment (and repression) of the cell cycle gene during SS. The gene is thereby maintained in a chromatin environment more suitable for low level expression and rapid reactivation in contrast with the chromatin environment closely associated to the NP (Shaklai et al., 2007).

Signaling mechanism initiating TFIIIC changes

What molecular trigger could be responsible for the observed behavior of TFIIIC upon SS? SS is a complicated stress situation for the cell and several signaling pathways are both activated and repressed (Pirkmajer and Chibalin, 2011). A recent study has reported the ability of Aurora-A to compete with TFIIIC for binding to N-MYC-regulated genes in S-phase (Buchel et al., 2017). These results invoke that post-translational modifications of TFIIIC, such as phosphorylation, might play a crucial role. Very intriguingly, the fourth-largest TFIIIC subunit (GTF3C4) contains a conserved serine residue (S611) which phosphorylation has been linked to a metastatic phenotype (Wang et al., 2010). Therefore, post-translational modifications of TFIIIC could be an appealing mechanism to discriminate among the numerous extra-TFIIIC Pol III functions and it deserves future investigation.

In conclusion, our study unveils a rapid and reversible TFIIIC- and AEs-dependent rewiring of genome topology acting on promoter-anchored chromatin loops and coupled with changes in H3K18ac of the associated AEs during SS. The 3D-genome reorganization enables the use of acetylated AEs and TFIIIC complexes as rescue-modules for correct nuclear positioning during SS to ultimately ensure steady state levels of expression of crucial cell cycle-regulated genes. Finally, as expression of these genes is found to predict clinical outcome of breast cancer patients (Figures S7I-S7K) and tumors have regions with poor blood supply and growth factor starvation (Anastasiou, 2017), our study could potentially illuminate new avenues to target post-translationally modified TFIIIC for clinical intervention.

Acknowledgments

We would like to thank all the members of the Beato's lab as well as members of the CRG Gene Regulation, Stem Cells and Cancer Program for the invaluable source of insight and helpful tips. We also thank the CRG Genome Facility as well as the 4D Genome Unit of the Synergy program, especially Yasmina Cuartero for her precious help with sequencing. We also thank Prof. Simone Ottonello (University of Parma) for his valuable suggestions, Davide Carnervali (University of Parma) for help with detecting AEs expressed in our cell line, and Jose Luis Villanueva (4D Genome Unit) for his help with mapping RNA-seq data.

Funding

Spanish Ministry of Economy and Competitiveness 'Centro de Excelencia Severo Ochoa 2013–2017' [SEV-2012-0208] and BFU2016-76141-P (to S.L.); ACER (to C.R.G.); EMBO Long-term Fellowship (ALTF 1201-2014 to R.F.); Marie Curie Individual Fellowship (H2020-MSCA-IF-2014); European Research Council under the European Union's Seventh Framework Programme (FP7/2007–2013/ERC Synergy grant agreement 609989 [4DGenome]). We acknowledge the support of the CERCA Programme / Generalitat de Catalunya. Funding for open access charge: European Research Council. We also acknowledge the support of the Italian Association for Cancer Research (AIRC, Grant IG16877 to G.D.).

Author Contributions

R.F. and L.I.L.C. and M.B. designed the experiments. R.F., L.I.L.C., C.D.V., A.L. and F.D.L. performed the experiments. R.F., Q.V., J.Q.O. carried out the biostatistics analysis. F.D.L. also assisted with the sequencing. R.F. and M.B. wrote the manuscript in consultation with G.D., M.T. and S.L. M.T. also provided some of the antibodies used in this study.

Declaration of Interests

None declared.

References

Anastasiou, D. (2017). Tumour microenvironment factors shaping the cancer metabolism landscape. Br J Cancer *116*, 277-286.

Bennett, E.A., Keller, H., Mills, R.E., Schmidt, S., Moran, J.V., Weichenrieder, O., and Devine, S.E. (2008). Active Alu retrotransposons in the human genome. Genome Res *18*, 1875-1883.

Boeynaems, S., Alberti, S., Fawzi, N.L., Mittag, T., Polymenidou, M., Rousseau, F., Schymkowitz, J., Shorter, J., Wolozin, B., Van Den Bosch, L.*, et al.* (2018). Protein Phase Separation: A New Phase in Cell Biology. Trends Cell Biol *28*, 420-435.

Bolzer, A., Kreth, G., Solovei, I., Koehler, D., Saracoglu, K., Fauth, C., Muller, S., Eils, R., Cremer, C., Speicher, M.R.*, et al.* (2005). Three-dimensional maps of all chromosomes in human male fibroblast nuclei and prometaphase rosettes. PLoS Biol *3*, e157.

Buchel, G., Carstensen, A., Mak, K.Y., Roeschert, I., Leen, E., Sumara, O., Hofstetter, J., Herold, S., Kalb, J., Baluapuri, A.*, et al.* (2017). Association with Aurora-A Controls N-MYC-Dependent Promoter Escape and Pause Release of RNA Polymerase II during the Cell Cycle. Cell Rep *21*, 3483-3497.

Chuong, E.B., Elde, N.C., and Feschotte, C. (2017). Regulatory activities of transposable elements: from conflicts to benefits. Nat Rev Genet *18*, 71-86.

Consortium, E.P. (2012). An integrated encyclopedia of DNA elements in the human genome. Nature *489*, 57-74.

Crepaldi, L., Policarpi, C., Coatti, A., Sherlock, W.T., Jongbloets, B.C., Down, T.A., and Riccio, A. (2013). Binding of TFIIIC to sine elements controls the relocation of activity-dependent neuronal genes to transcription factories. PLoS Genet *9*, e1003699.

Dieci, G., Fiorino, G., Castelnuovo, M., Teichmann, M., and Pagano, A. (2007). The expanding RNA polymerase III transcriptome. Trends Genet *23*, 614-622.

Donze, D. (2012). Extra-transcriptional functions of RNA Polymerase III complexes: TFIIIC as a potential global chromatin bookmark. Gene *493*, 169-175.

Engelen, E., Brandsma, J.H., Moen, M.J., Signorile, L., Dekkers, D.H., Demmers, J., Kockx, C.E., Ozgur, Z., van, I.W.F., van den Berg, D.L.*, et al.* (2015). Proteins that bind regulatory regions identified by histone modification chromatin immunoprecipitations and mass spectrometry. Nat Commun *6*, 7155.

Ferrari, R., Gou, D., Jawdekar, G., Johnson, S.A., Nava, M., Su, T., Yousef, A.F., Zemke, N.R., Pellegrini, M., Kurdistani, S.K.*, et al.* (2014). Adenovirus small E1A employs the lysine acetylases p300/CBP and tumor suppressor Rb to repress select host genes and promote productive virus infection. Cell Host Microbe *16*, 663-676.

Ferrari, R., Pellegrini, M., Horwitz, G.A., Xie, W., Berk, A.J., and Kurdistani, S.K. (2008). Epigenetic reprogramming by adenovirus e1a. Science *321*, 1086-1088.

Ferrari, R., Rivetti, C., Acker, J., and Dieci, G. (2004). Distinct roles of transcription factors TFIIIB and TFIIIC in RNA polymerase III transcription reinitiation. Proc Natl Acad Sci U S A *101*, 13442-13447.

Finlan, L.E., Sproul, D., Thomson, I., Boyle, S., Kerr, E., Perry, P., Ylstra, B., Chubb, J.R., and Bickmore, W.A. (2008). Recruitment to the nuclear periphery can alter expression of genes in human cells. PLoS Genet *4*, e1000039.

Galli, G.G., Carrara, M., Francavilla, C., de Lichtenberg, K.H., Olsen, J.V., Calogero, R.A., and Lund, A.H. (2013). Genomic and proteomic analyses of Prdm5 reveal interactions with insulator binding proteins in embryonic stem cells. Mol Cell Biol *33*, 4504-4516.

Gu, Z., Jin, K., Crabbe, M.J., Zhang, Y., Liu, X., Huang, Y., Hua, M., Nan, P., Zhang, Z., and Zhong, Y. (2016). Enrichment analysis of Alu elements with different spatial chromatin proximity in the human genome. Protein Cell *7*, 250-266.

Hiraga, S., Botsios, S., Donze, D., and Donaldson, A.D. (2012). TFIIIC localizes budding yeast ETC sites to the nuclear periphery. Mol Biol Cell *23*, 2741-2754.

Ji, X., Dadon, D.B., Abraham, B.J., Lee, T.I., Jaenisch, R., Bradner, J.E., and Young, R.A. (2015). Chromatin proteomic profiling reveals novel proteins associated with histone-marked genomic regions. Proc Natl Acad Sci U S A *112*, 3841-3846.

Jin, Q., Yu, L.R., Wang, L., Zhang, Z., Kasper, L.H., Lee, J.E., Wang, C., Brindle, P.K., Dent, S.Y., and Ge, K. (2011). Distinct roles of GCN5/PCAF-mediated H3K9ac and CBP/p300-mediated H3K18/27ac in nuclear receptor transactivation. EMBO J *30*, 249-262.

Jourdain, S., Acker, J., Ducrot, C., Sentenac, A., and Lefebvre, O. (2003). The tau95 subunit of yeast TFIIIC influences upstream and downstream functions of TFIIIC.DNA complexes. J Biol Chem *278*, 10450-10457.

Kramerov, D.A., Grigoryan, A.A., Ryskov, A.P., and Georgiev, G.P. (1979). Long double-stranded sequences (dsRNA-B) of nuclear pre-mRNA consist of a few highly abundant classes of sequences: evidence from DNA cloning experiments. Nucleic Acids Res *6*, 697-713.

Kundu, T.K., Wang, Z., and Roeder, R.G. (1999). Human TFIIIC relieves chromatin-mediated repression of RNA polymerase III transcription and contains an intrinsic histone acetyltransferase activity. Mol Cell Biol *19*, 1605-1615.

Le Dily, F., Bau, D., Pohl, A., Vicent, G.P., Serra, F., Soronellas, D., Castellano, G., Wright, R.H., Ballare, C., Filion, G.*, et al.* (2014). Distinct structural transitions of chromatin topological domains correlate with coordinated hormone-induced gene regulation. Genes Dev *28*, 2151-2162.

Le Dily, F., and Beato, M. (2018). Signaling by Steroid Hormones in the 3D Nuclear Space. Int J Mol Sci *19*.

Lee, T.I., and Young, R.A. (2013). Transcriptional regulation and its misregulation in disease. Cell *152*, 1237-1251.

Li, L., Lyu, X., Hou, C., Takenaka, N., Nguyen, H.Q., Ong, C.T., Cubenas-Potts, C., Hu, M., Lei, E.P., Bosco, G.*, et al.* (2015). Widespread rearrangement of 3D chromatin organization underlies polycomb-mediated stress-induced silencing. Mol Cell *58*, 216-231.

Male, G., von Appen, A., Glatt, S., Taylor, N.M., Cristovao, M., Groetsch, H., Beck, M., and Muller, C.W. (2015). Architecture of TFIIIC and its role in RNA polymerase III pre-initiation complex assembly. Nat Commun *6*, 7387.

McLean, C.Y., Bristor, D., Hiller, M., Clarke, S.L., Schaar, B.T., Lowe, C.B., Wenger, A.M., and Bejerano, G. (2010). GREAT improves functional interpretation of cis-regulatory regions. Nat Biotechnol *28*, 495-501.

Mehta, I.S., Amira, M., Harvey, A.J., and Bridger, J.M. (2010). Rapid chromosome territory relocation by nuclear motor activity in response to serum removal in primary human fibroblasts. Genome Biol *11*, R5.

Mertens, C., and Roeder, R.G. (2008). Different functional modes of p300 in activation of RNA polymerase III transcription from chromatin templates. Mol Cell Biol *28*, 5764-5776.

Moqtaderi, Z., Wang, J., Raha, D., White, R.J., Snyder, M., Weng, Z., and Struhl, K. (2010). Genomic binding profiles of functionally distinct RNA polymerase III transcription complexes in human cells. Nat Struct Mol Biol *17*, 635-640.

Ostapcuk, V., Mohn, F., Carl, S.H., Basters, A., Hess, D., Iesmantavicius, V., Lampersberger, L., Flemr, M., Pandey, A., Thoma, N.H.*, et al.* (2018). Activity-dependent neuroprotective protein recruits HP1 and CHD4 to control lineage-specifying genes. Nature *557*, 739-743.

Pascali, C., and Teichmann, M. (2013). RNA polymerase III transcription - regulated by chromatin structure and regulator of nuclear chromatin organization. Subcell Biochem *61*, 261-287.

Pirkmajer, S., and Chibalin, A.V. (2011). Serum starvation: caveat emptor. Am J Physiol Cell Physiol *301*, C272-279.

Poljsak, B., and Milisav, I. (2012). Clinical implications of cellular stress responses. Bosn J Basic Med Sci *12*, 122-126.

Ringner, M., Fredlund, E., Hakkinen, J., Borg, A., and Staaf, J. (2011). GOBO: gene expression-based outcome for breast cancer online. PLoS One *6*, e17911.

Ruiz-Velasco, M., Kumar, M., Lai, M.C., Bhat, P., Solis-Pinson, A.B., Reyes, A., Kleinsorg, S., Noh, K.M., Gibson, T.J., and Zaugg, J.B. (2017). CTCF-Mediated Chromatin Loops between Promoter and Gene Body Regulate Alternative Splicing across Individuals. Cell Syst *5*, 628-637 e626.

Santos, A., Wernersson, R., and Jensen, L.J. (2015). Cyclebase 3.0: a multi-organism database on cell-cycle regulation and phenotypes. Nucleic Acids Res *43*, D1140-1144.

Shaklai, S., Amariglio, N., Rechavi, G., and Simon, A.J. (2007). Gene silencing at the nuclear periphery. FEBS J *274*, 1383-1392.

Stadhouders, R., Vidal, E., Serra, F., Di Stefano, B., Le Dily, F., Quilez, J., Gomez, A., Collombet, S., Berenguer, C., Cuartero, Y.*, et al.* (2018). Transcription factors orchestrate dynamic interplay between genome topology and gene regulation during cell reprogramming. Nat Genet.

Su, M., Han, D., Boyd-Kirkup, J., Yu, X., and Han, J.D. (2014). Evolution of Alu elements toward enhancers. Cell Rep *7*, 376-385.

Van Bortle, K., and Corces, V.G. (2012). tDNA insulators and the emerging role of TFIIIC in genome organization. Transcription *3*, 277-284.

van de Werken, H.J.G., Haan, J.C., Feodorova, Y., Bijos, D., Weuts, A., Theunis, K., Holwerda, S.J.B., Meuleman, W., Pagie, L., Thanisch, K.*, et al.* (2017). Small chromosomal regions position themselves autonomously according to their chromatin class. Genome Res *27*, 922-933.

Vihervaara, A., Mahat, D.B., Guertin, M.J., Chu, T., Danko, C.G., Lis, J.T., and Sistonen, L. (2017). Transcriptional response to stress is pre-wired by promoter and enhancer architecture. Nat Commun *8*, 255.

Wang, H., La Russa, M., and Qi, L.S. (2016). CRISPR/Cas9 in Genome Editing and Beyond. Annu Rev Biochem *85*, 227-264.

Wang, S., Sun, H., Ma, J., Zang, C., Wang, C., Wang, J., Tang, Q., Meyer, C.A., Zhang, Y., and Liu, X.S. (2013). Target analysis by integration of transcriptome and ChIP-seq data with BETA. Nat Protoc *8*, 2502-2515.

Wang, Y.T., Tsai, C.F., Hong, T.C., Tsou, C.C., Lin, P.Y., Pan, S.H., Hong, T.M., Yang, P.C., Sung, T.Y., Hsu, W.L.*, et al.* (2010). An informatics-assisted label-free quantitation strategy that depicts phosphoproteomic profiles in lung cancer cell invasion. J Proteome Res *9*, 5582-5597.

Weintraub, A.S., Li, C.H., Zamudio, A.V., Sigova, A.A., Hannett, N.M., Day, D.S., Abraham, B.J., Cohen, M.A., Nabet, B., Buckley, D.L.*, et al.* (2017). YY1 Is a Structural Regulator of Enhancer-Promoter Loops. Cell *171*, 1573-1588 e1528.

Figure Legends

Figure 1. TFIIIC occupancy at AEs increased during SS in breast cancer cells.

(A) Venn diagram of overlapping peaks of CTCF (*top panel*) and TFIIIC (*bottom panel*) in +S and –S conditions.

(B) Staked plot for CTCF peaks (*left panel*) and TFIIIC peaks (*right panel*) over AEs, tRNA or other loci in the presence (+S) or absence of serum (-S).

(C) Heatmap showing a 10 kb window (±5 kb) around the TFIIIC or CTCF peaks in the presence (+S) or absence (–S) of serum (plotted is the -log10 of the Poisson p-value; color bar scale, with increasing shades of color, stands for higher enrichment). For TFIIIC, enrichments in the +S and –S samples are on the right. Pearson's correlation coefficients are shown for the indicated comparisons.

(D) Genome browser view of representative loci of the two ChIP-seq replicates for the Pol III machinery - BDP1, TFIIIC and Pol III (RPC39) - and for CTCF. Reported are also the UCSC genome browser tracks of tRNA genes and AEs. TFIIIC bound to AEs is highlighted by grey rectangles. The corresponding genes and the direction of transcription (arrow) are shown at the bottom.

(E) Fraction of TFIIIC peaks relative to the distance to all human TSSs as calculated by GREAT, in +S and –S.

Figure 2. TFIIIC occupancy at AEs near TSS of Pol II transcribed genes during SS in various cell lines.

(A) Genome browser view of representative *HELLS* locus with ChIP-seq data for TFIIIC in T47D with the additional representation of the genomic profile of TFIIIC occupancy in other cell lines subjected to SS. Highlighted in grey is the AE bound by TFIIIC in the 4 cell lines. The corresponding gene and the direction of transcription (arrow) are shown at the bottom.

(B) Matrix of Pearson's correlation coefficients of TFIIIC ChIP-seq data across the cell lines indicated. Color scale is shown.

(C and D) CEAS plots of TFIIIC average binding in conditions of +S, –S and –S followed by serum addition for 30 min for T47D (C) and T98G (D) cells; the graphs are plotted over those peaks detected in the -S condition (plotted is the –log10 of the Poisson p-value).

Figure 3. H3K18ac and transcription of Pol II promoters with AEs bound by TFIIIC.

(A and B) Heatmaps of TFIIIC (A) and H3K18ac (B) enrichment across TAPs ranked for significant occupancy by TFIIIC in condition of –S (both conditions +S and –S are shown) spanning a 10 kb region (±5 kb). Color bar scales with increasing shades of color stand for higher enrichment (plotted is the –log10 of the Poisson p-value).

(C) Genome browser view of representative *MCM2* locus with ChIP-seq data for the Pol III machinery (TFIIIC, BDP1 and Pol III), CTCF and Pol II. The graph also shows the tracks for total RNA-seq in the two conditions (+S and –S) and the UCSC genome browser track of AEs. The TFIIIC-bound AE is highlighted by a grey rectangle. *MCM2* gene and its direction of transcription

(arrow) are shown at the bottom. Note that upon SS, TFIIIC recruitment to the AEs is observed in all cell lines analyzed, which is accompanied by increased H3K18ac restricted to the AE bound by TFIIIC.

(D and E) CEAS profile of H3K18ac enrichment in +S and –S conditions across all AEs (D) or tRNA (E) bound by TFIIIC in –S (plotted is the –log10 of the Poisson p-value).

(F and G) Venn diagrams showing the total number of AEs bound by TFIIIC and acetylated in H3K18 (F) and the TAPs acetylated in H3K18 (G).

(H) Boxplot of RNA expression in +S or -S conditions for TAPs or a random dataset of the same size. Two-tailed paired Student's *t*-test in pairwise comparisons, **p-value < 0.001.

Figure 4. Gene expression changes upon SS and effect of TFIIIC depletion.

(A-B) Scatter plot of gene expression comparing conditions of +S *vs* –S and siGTF3C5 *vs* the –S condition in T47D. The number of genes up- or down-regulated (FC> 1.5; p-value < 0.05) is indicated in red or blue, respectively. The reproducibility of replicated samples in A and B is shown in Figure S4A. GTF3C5 silencing levels are shown in Figure S4D. Analysis of differential gene expression of siGTF3C5 *vs* siCTRL in the –S condition is shown in Figure S4E. The changes induced by the expression of the siCTRL when compared to –S (non-transfected cells) are shown in Figure S4F.

(C) Heatmaps of gene expression for siGTF3C5 and siCTRL cells (both in –S) *vs* –S. Only the genes that changed their expression significantly in the siGTF3C5-cells, and not in the siCTRL

cells are shown. Two classes of genes were designated as TFIIIC-activated genes (TAGs) or TFIIIC-repressed genes (TRGs).

(D) ChIP-qPCR for H3K18ac enrichment at two AEs bound by TFIIIC in SS (*UHRF1* and *HELLS* loci) for the different conditions indicated.

(E) mRNA-seq expression analysis after serum exposure for the indicated times for TAGs in conditions of siCTRL and siGTF3C5 in T47D cells. Significant p-values from a two-tailed paired Student's *t*-test are reported. *** $p < 1.0E10^{-20}$, ** $p < 1.0E10^{-12}$. The statistical comparison between 0 to 3 h in siCTRL cells is shown to highlight the rapidity of gene activation after serum addition. GTF3C5 depleted levels were maintained during the time course (Figure S4N). *PPIA*, used as a control gene, did respond neither to siGTF3C5 nor to serum (Figure S4O).

(H) Venn Diagram of the overlap between TAGs (according to Figure 4C) and TAPs (according to Figure 3A).

Figure 5. TFIIIC increases its interaction with CTCF bound to promoters of genes affected by TFIIIC knock down upon SS.

(A) Hi-C analysis of TFIIIC contacts represented as log2 FC (and 95 % CI) of the TFIIIC-promoter contact enrichment between +S and -S conditions for genes changing (orange) and not changing (green) upon SS. PPr = 0.93 indicates a high probability of an increase TFIIIC contacts with promoters of genes whose expression changed upon SS (compared to promoters of genes whose expression did not change).

(B) Heatmaps of CTCF and Pol II enrichment in T47D across all human TSSs spanning a 10 kb region (±5 kb) in +S and –S condition. Boxes represent different clusters of enrichment as calculated by hierarchical clustering. Color bar scales with increasing shades indicate higher enrichment (plotted is the –log10 of the Poisson p-value).

(C) Co-immunoprecipitation of CTCF and TFIIIC in T47D comparing +S and –S conditions ("beads only" are used as a control). Membranes were probed with anti-CTCF and GTF3C2 antibodies. Loading inputs for both proteins are also showed.

(D) Hi-C analysis of TFIIIC and CTCF contacts represented as log2 FC (and 95 % CI) of the specific CTCF-TFIIIC contact enrichment compared to CTCF and TFIIIC additive effect for both +S and -S conditions. (E=expected by CTCF and TFIIIC additive effect). PPr = 0.83 indicates a high probability of an increase in TFIIIC Hi-C contact with CTCF the -S sample compared to +S.

Figure 6. Long-range interactions of TFIIIC-mediated DNA looping participate in maintaining gene expression patterns during SS.

(A and B) Hi-C interaction matrixes of two representative loci (*UHRF1 and CCNF*, respectively) of genes down-regulated by siGTF3C5. Genomic loops between the AE bound by TFIIIC and its respective targets are indicated by arrows (middle panels) in the subtraction matrix (+S matrix is subtracted by the –S matrix) represented above (top panel). The regions with changes in their interaction upon SS have been zoomed out to better visualize those regions of preferred interaction (top panel). ChIP-seq and RNA-seq data (A and B indicate two biological replicates)

are also reported as genome browser views of the two loci (bottom panel). Grey rectangles highlight the position of the AEs and the genes interacting.

(C) Virtual 4C of the *CCNF* locus for the +S and –S conditions (red and grey respectively). The peak with increased Hi–C contacts between the AE and the *CCNF* promoter is indicated by an arrow. Grey rectangles highlight the position of the AE and the genes interacting.

(D) Venn diagram of overlap between TAGs (613 genes) and 193 genes bound by TFIIIC directly (within a 10 kb region) or via DNA looping (see main text).

(E) Heatmaps of the expression of the genes resulting from the analysis in Figure 6D for conditions of +S, siGTF3C5 and siCTRL all compared to cells in the absence of serum (-S).

(F) Boxplot of CTCF significant binding events within a 10 kb region around the TSS of the 193 genes shown in Figure 6D, or a random dataset of TSS of the same size. P-value of a Friedman X^2 test is indicated.

Figure 7. DNA looping at cell cycle genes is impaired by TFIIIC knock down.

(A) TFIIIC enrichment within Hi-C data in the –S condition of the TAGs and TRGs. Higher significant TFIIIC enrichment for TAGs (those genes down-regulated by siGTF3C5). P-value for logistic regression comparing TAGs and TAPs is reported.

(B) Log2 FC (and 95 % CI) of the specific intra-TADs contacts made by TFIIIC in +S/-S or siGTF3C5/siCTRL cells. siGTF3C5/siCTRL Hi-C data show significant (PPr =0.99) decrease of total intra-TADs contacts compared to –S/siCTRL.

(C) Hi-C subtraction matrix of the *UHRF1* locus for siCTRL and siGTF3C5 cells. The siGTF3C5 matrix is subtracted of the siCTRL matrix. Arrows indicate the looping between the AE bound by TFIIIC and its respective targets (*PLIN4/5* or *UHRF1*). Each of the regions that change their interaction upon SS has been zoomed out to better visualize the regions of preferred interactions.

(D) Boxplot of the normalized interaction score of Hi-C data for siCTRL and siGTF3C5 between promoters and TFIIIC-bound AEs for the 193 genes regulated by TFIIIC shown in Figure 6D. Two Hi-C biological replicates were used (p-value from Friedman X^2 test is indicated).

(E) *UHRF1* expression by qRT-PCR in T47D parental cells (WT) and Alu-CRISPR/Cas9-Clon11 in the absence of serum (mean ± SEM of 2 biological replicates; data in WT cells have been normalized to 1). One Tail T-test p-value is indicated.

(F) FISH staining of the *CCNF* locus (red) in T47D cells in +S and –S conditions, and siCTRL and siGTF3C5 cells in the absence of serum. DNA is counterstained with DAPI (blue). White arrows indicate the position of the *CCNF* locus. Scale bar is indicated.

(G) Boxplot quantification of the radial distance of *CCNF* probes from the NP. ***p-value from two-tail unpaired Student's *t*-test.

(H) Schematic model of TFIIIC action in DNA looping in response to SS. See text for description.

Supplementary Figure Legends

Supplementary Figure S1. TFIIIC, but not CTCF, occupancy to AEs and tRNA genes is altered upon SS.

(A) Schematic view of experimental design.

(B) FACS analysis showing the percentage of T47D cells at the indicated phases of the cell cycle.

(C) Word cloud analysis of repetitive elements bound by TFIIIC in the presence (+S) or absence (-S) serum.

(D) Proportional Venn diagram of total AEs bound by TFIIIC detected in SS *vs* ETC sites (with only B-box).

(E) Boxplot of normalized significant counts for TFIIIC (upper) and CTCF (bottom) mapping at tRNA genes in condition of +S and -S.

(F) Boxplot of normalized significant counts for TFIIIC and CTCF mapping at AEs in condition of +S and -S.

(G) Chromosomal enrichment for TFIIIC ChIP-seq occupancy in +S as calculated by CEAS.

(H) Chromosomal enrichment for TFIIIC ChIP-seq occupancy in –S as calculated by CEAS. (see CEAS package in STAR Methods). Reported for each condition are the chromosome ChIP enrichment *vs* the genome control and the corresponding p-value.

(I) CEAS plots of BDP1 or Pol III average binding to tRNA genes in condition of +S and -S (plotted is the –log10 of the Poisson p-value).

(J) CEAS plots of BDP1 or Pol III (right) average binding to AEs in condition of +S and -S (plotted is the –log10 of the Poisson p-value).

(K) Genome browser view of representative *7SLRNA* locus (red box) with ChIP-seq data for Pol III, BDP1 and TFIIIC in T47D in +S and –S conditions. Note how TFIIIC occupies a more downstream region compared to the 5'-end of the *7SLRNA* gene occupied by Pol III and BDP1.

Supplementary Figure S2. TFIIIC binding in different cell lines shows increased AEs occupancy upon SS.

(A) Bar plot for all TFIIIC peaks detected in +S and –S condition of all the 4 different cell lines tested.

(B) CEAS plot of TFIIIC average binding in condition of +S and –S over peaks detected in the -S condition in MCF10A cells (plotted is the –log10 of the Poisson p-value). The enrichment in peaks corresponds to AEs.

(C) Genome browser view of representative *CCNE1, MDM4 and UBE2V2* loci with ChIP-seq data for Pol III, BDP1 and TFIIIC in MCF10A and T47D breast cell lines. The graph includes the tracks for AEs and tRNA genes in +S and –S conditions. Highlighted in grey is the AE bound by TFIIIC in the two cell lines close to the TSS of the genes indicated.

(D and E) CEAS plots of TFIIIC average binding in condition of +S and –S over peaks detected in -S condition for T98G and IMR90, respectively. The peaks in -S are enriched in AEs in the two cell lines (not shown).

Supplementary Figure 3. GO enrichment, motif analysis and Pol II occupancy of TAPs.

(A) Bar plots of GO terms enrichment of TAPs. GO terms are ranked from the lowest to the highest p-value of the first nine terms found by DAVID.

(B) Motif analysis (Seqpos tool) for TAPs.

(C) Heatmap of AE density across all human TSS spanning a 6 kb region (±3 kb), and sorted by high to low AE density. TAPs correspond to those Pol II promoters with TFIIIC-bound. Color bar scale with increasing shades of color stands for higher AE density.

(D) Heatmaps spanning a 10 kb region (±5 kb) of Pol II enrichment across TAPs (+S and –S conditions are shown). Color bar scales with increasing shades of color stand for higher enrichment (plotted is the –log10 of the Poisson p-value).

(E) Boxplot of normalized counts for Pol II enrichment over TAPs in Figure S3D. P-value for a two-tailed heteroscedastic *t*-test is reported.

(F) Boxplot of expression of all intergenic AEs (see text) in +S or -S conditions. P-value for a two-tailed paired Student's *t*-test is reported.

Supplementary Figure 4. Global Gene expression analysis of T47D before and after SS and in condition of TFIIIC depletion.

(A) Principal component analysis for mRNA-seq of T47D cells in the presence or absence of serum (+/-S) and T47D cells transfected with siGTF3C5 or siCTRL, in +/-S conditions. The two replicates used for each condition are shown. The replicate samples show reproducibility and clear differences between the samples.

(B and C) Bar plots of GO enrichment for list of genes up-regulated and down-regulated in Figure 4A (according to GOC).

(D) Immunoblot probing the levels of GTF3C5 for cells transfected with siGTF3C5 or control siCTRL.

(E) Volcano plot for comparing mRNA-seq of siGTF3C5 *vs* siCTRL in -S conditions (plotted the –log10 of the p-value *vs* the -log2 ratio of siGTF3C5 *vs* siCTRL). The genes that scored significant (FC>1.5; p-value < 0.05) are indicated in red. *GTF3C5* is found among the most downregulated genes.

(F) Scatter plot of gene expression comparing siCTRL treated cells (-S) *vs* –S condition. The number of genes up- or down-regulated (FC > 1.5; p-value < 0.05) are indicated in red or blue, respectively.

(G and H) BETA analysis for TFIIIC binding in SS and the gene expression profile of siGTF3C5 (G) and siCTRL (H) cells in -S conditions (p-values are indicated). TFIIIC binding in SS only significantly correlated with downregulated genes upon its silencing.

(I and J) Bar plots of GO enrichment, as calculated by DAVID, for TAGs and TRGs in siGTF3C5 cells, respectively (according to Figure 4C).

(K) Genome browser view of representative *HELLS* and *MCM7* loci. ChIP-seq data of CTCF, TFIIIC and Pol II in T47D for +S and -S conditions is represented. Additionally, the TFIIIC occupancy in T98G, MCF10A and IMR90 is also shown. Tracks for RNA expression of T47D in the +S and –S conditions for non-transfected, and for siCTRL and siGTF3C5 in -S are included.

In all cases, A and B indicate two biological replicates. Highlighted in grey is the AE bound by TFIIIC in all 4 cell lines close to the TSS of the *HELLS* and *MCM7* loci.

(L) Cell cycle profile of +S, siCTRL or siGT3C5 cells in –S condition (dotted lines represent reference values of the siCTRL).

(M) Sitepro profile of T47D tRNA-seq enrichment in +S or –S conditions across all tRNA genes spanning a 400 bp region (±200 bp; plotted is the average expression in RPM). A reduction in tRNA expression is observed upon SS, which is not significantly different from that obtained in siGTF3C5 cells.

(N and O) qRT-PCR expression analysis of *GTF3C5* (N) and *PPIA* (O) in T47D cells (siCTRL and siGT3C5) released from SS by serum addition for the indicated times. Graph represents the mean ± SEM from two biological experiments, in which the value in siCTRL cells was arbitrarily set as 1 at each time point. Note that the knockdown of the Pol III factor always reaches values of more than 70% at each time point analyzed. Moreover, serum exposure had no effect on the kinetic of a control gene *PPIA* that is neither affected by the SS or by the siGTF3C5 (Table S5).

(P) DAVID GO enrichment of the overlapping genes shown in Figure 4J.

Supplementary Figure 5. Interaction of TFIIIC and CTCF is not dependent on the expression levels of TFIIIC

Western blot of different TFIIIC subunits (GTF3C1, GTF3C2, GTF3C4 and GTF3C5) in +S and –S conditions. For each panel, a loading control with Tubulin is also shown.

Supplementary Figure 6. Interaction of TFIIIC and CTCF might generate a hyper-acetylated environment by acetylating H3K18 at TAPs upon SS and at looped genes.

(A) Genome browser view of representative cell cycle-related genes, *CCND1, CCNF, CENPE and POLQ*, for ChIP-seq data of CTCF and TFIIIC in T47D in +S and –S conditions. Highlighted with grey boxes are the multiple CTCF peaks. Note that multiple CTCF binding sites are present at the 5' end of the *CCNF* gene (see text). Transcription directionality is indicated.

(B) Sitepro plot of H3K18ac average at the TSS (±3 kb) of all human genes in +S or –S conditions in T47D cells (plotted is the –log10 of the Poisson p-value).

(C) Heatmap representation of H3K18ac spanning a 20 kb region of all human promoters in +S and –S conditions in T47D cells. Biased clustering show promoters that increased H3K18ac upon SS; this cluster contains several looped genes identified in the analysis from Figure 6D. The presence of *MYC*, whose expression is decreased upon SS, is shown in the cluster with H3K18ac on TSSs but not enhanced upon SS.

(D) Stacked plot of percentage of promoters bound by TFIIIC (both directly or through looping) which show changes in H3K18ac upon SS. Note that around 70% of them display increased acetylation.

(E) Genome browser view of representative *HSPG2, ZBTB40, CEP78* and *PSAT1* loci with ChIP-seq data for H3K18ac, TFIIIC and Pol II in T47D. Additionally, the genomic profile of TFIIIC occupancy in T98G, MCF10A and IMR90 is represented. The graph also includes the tracks for RNA expression of T47D in +S and –S conditions. Grey rectangles highlight the position of the

AEs close to the TSS of the TFIIIC-bound genes, and the black arrows indicate the corresponding interacting genes. Green rectangles represent genes affected by SS.

(F and G) Virtual 4C representation of the genes in panel E for the +S and –S conditions (red and blue, respectively). The viewpoint of the virtual 4C is the AE bound by TFIIIC. Arrows point to the location of the genes and the changes in normalized interaction frequency.

Supplementary Figure 7. TFIIIC ablation and AE deletion affects DNA looping and expression of distal UHRF1 locus.

(A) Virtual 4C of the *UHRF1* locus for the +S, –S conditions, siCTRL and siGTF3C5 cells (black and red arrows indicate the up- and downstream loops, respectively).

(B) Schematic representation of the CRISPR-Cas9 approach to delete the TFIIIC-bound AE located between the *PLIN4/5* and *UHRF1* loci in chromosome 17. The targeted AE is shown as a purple box. The position of the guide RNAs (gRNA1 and gRNA2, see STAR Methods for details) is shown. The wild-type (WT) and the deleted allele are shown. Arrows indicate the chromatin interactions in +S and -S conditions (red and black, respectively).

(C) PCR result for the screen of CRISPR-Cas9 T47D clones with primers Up3 and Down (see STAR Methods for details): the upper band corresponds to the WT allele, whereas the lower band correspond to the deleted allele. Almost all clones analyzed were heterozygous for the deletion. For further analysis, we selected Cln11. The size of DNA marker size is shown. * indicates a non-specific band. NC corresponds to no the no DNA sample.

(D) Boxplot quantification of the radial distance of *CCNF* probes from the NP for cells in the indicated conditions. P-values are for a two-tailed unpaired Student's *t*-test in pair-wise comparisons.

(E) Pie chart showing the classes of RE enriched in the published dataset of ADPN ChIP-seq (Consortium, 2012). AEs are indicated as black-boxed yellow slice.

(F) Sitepro profile of ADNP (Consortium, 2012) enrichment over TAPs-AEs, all TFIIIC-bound AEs and the 193 AEs that showed looping properties (Figure 6D). Worth of notice the increased enrichment of ADNP at looped AEs.

(G) Pie chart showing the percentage of mouse Adnp peaks belonging to RE and non-RE (GSE97945). Notice that almost all the binding of this factor lays on RE.

(H) Pie chart showing the percentage of RE peaks of mouse Adnp belonging to B-elements (mouse Alu-like SINE) (B1, B2, B3 and B4) compared to other elements. 50% of the bound REs are *bona fide* B elements.

(J and K) Kaplan–Meier plots of breast tumor samples. TAPs expression as shown in Figure 3A (J) or TAGs expression as shown in Figure 4C (K), respectively, was divided in three main groups according to their expression (with blue being the highest, red the intermediate and grey the lowest). P-values from a Mantel-Cox test are indicated. Higher expression of genes bound by TFIIIC or down-regulated by siGTF3C5 in T47D are associated with poor prognosis for overall survival and distance metastasis free survival (DMFS), respectively. Plots are generated using “Gene expression-based Outcome for Breast Cancer Online”.

(I) Boxplots of expression from tumors samples across the three breast cancer grades (GOBO) (Ringner et al., 2011) for TAGs. Boxplots are generated by using GOBO. TAGs have higher expression in most aggressive tumors (grade 3). P-value for the analysis is also indicated.

Figure 1


A
CTCF
−S
1033
32068
7746
+S
TFIIIC
−S
138
250
3012
+S

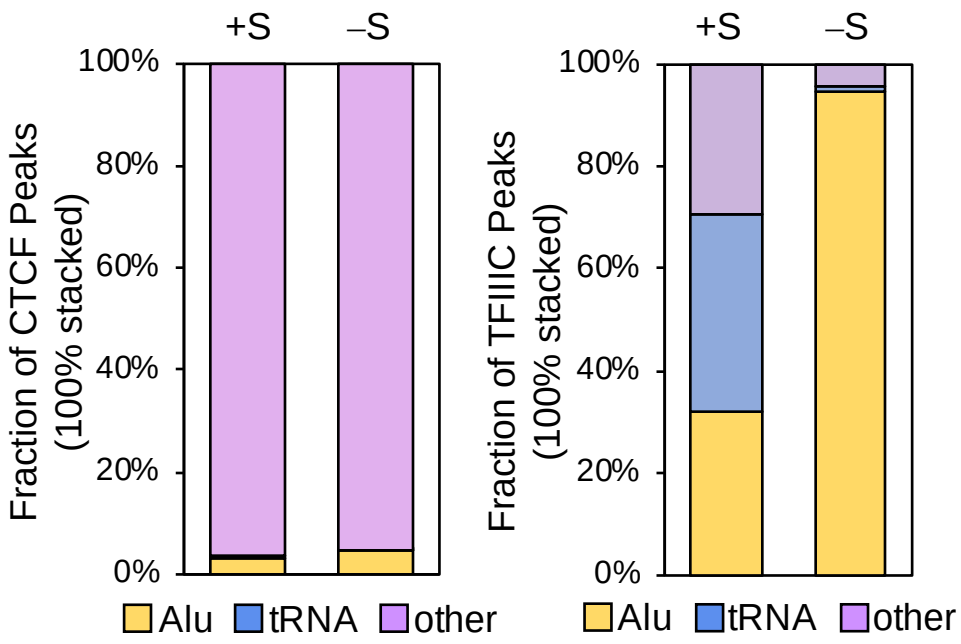
B
+S
−S
100%
80%
60%
40%
20%
0%
Fraction of CTCF Peaks (100% stacked)
Alu
tRNA
other
Fraction of TFIIIC Peaks (100% stacked)

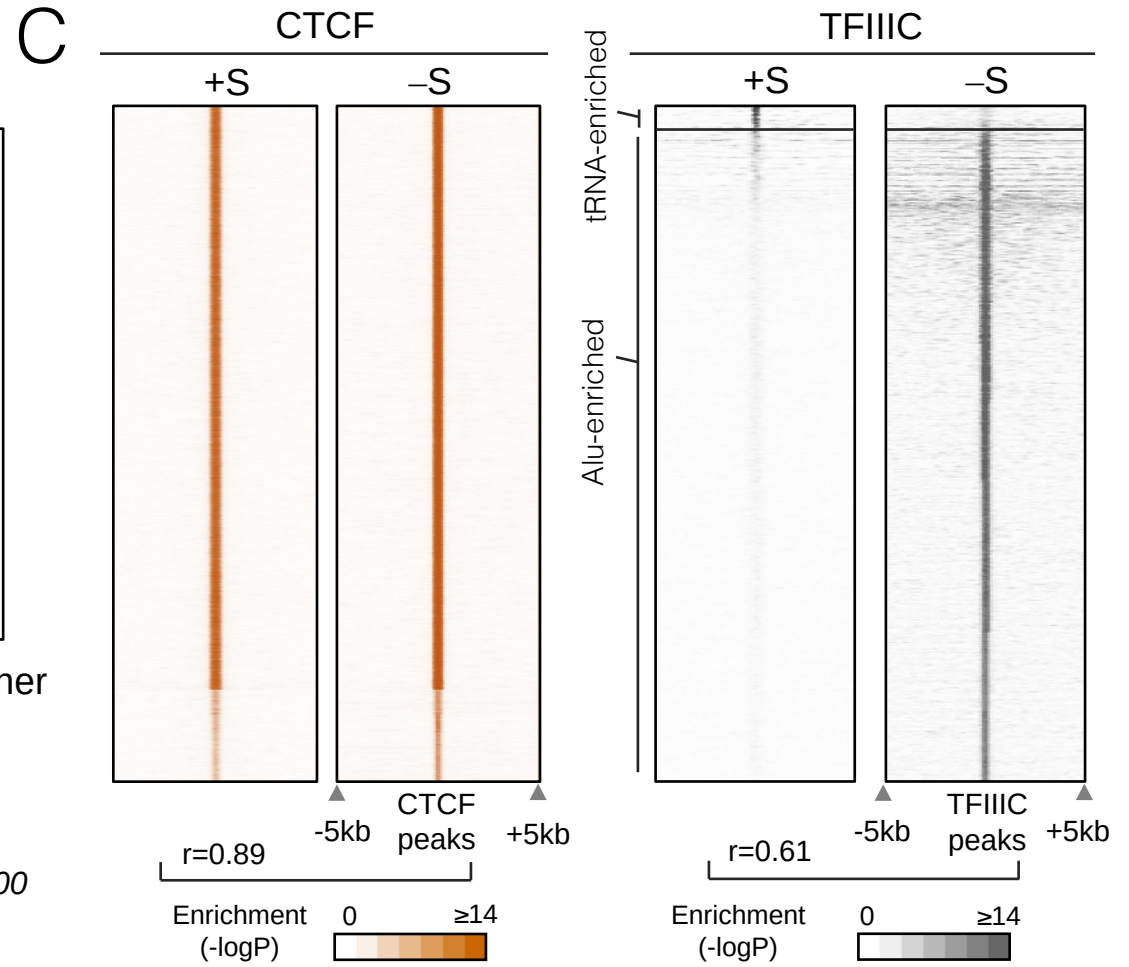
C
CTCF
+S
−S
-5kb
CTCF peaks
+5kb
r=0.89
Enrichment (-logP)
0
≥14
TFIIIC
tRNA-enriched
Alu-enriched
TFIIIC peaks
r=0.61

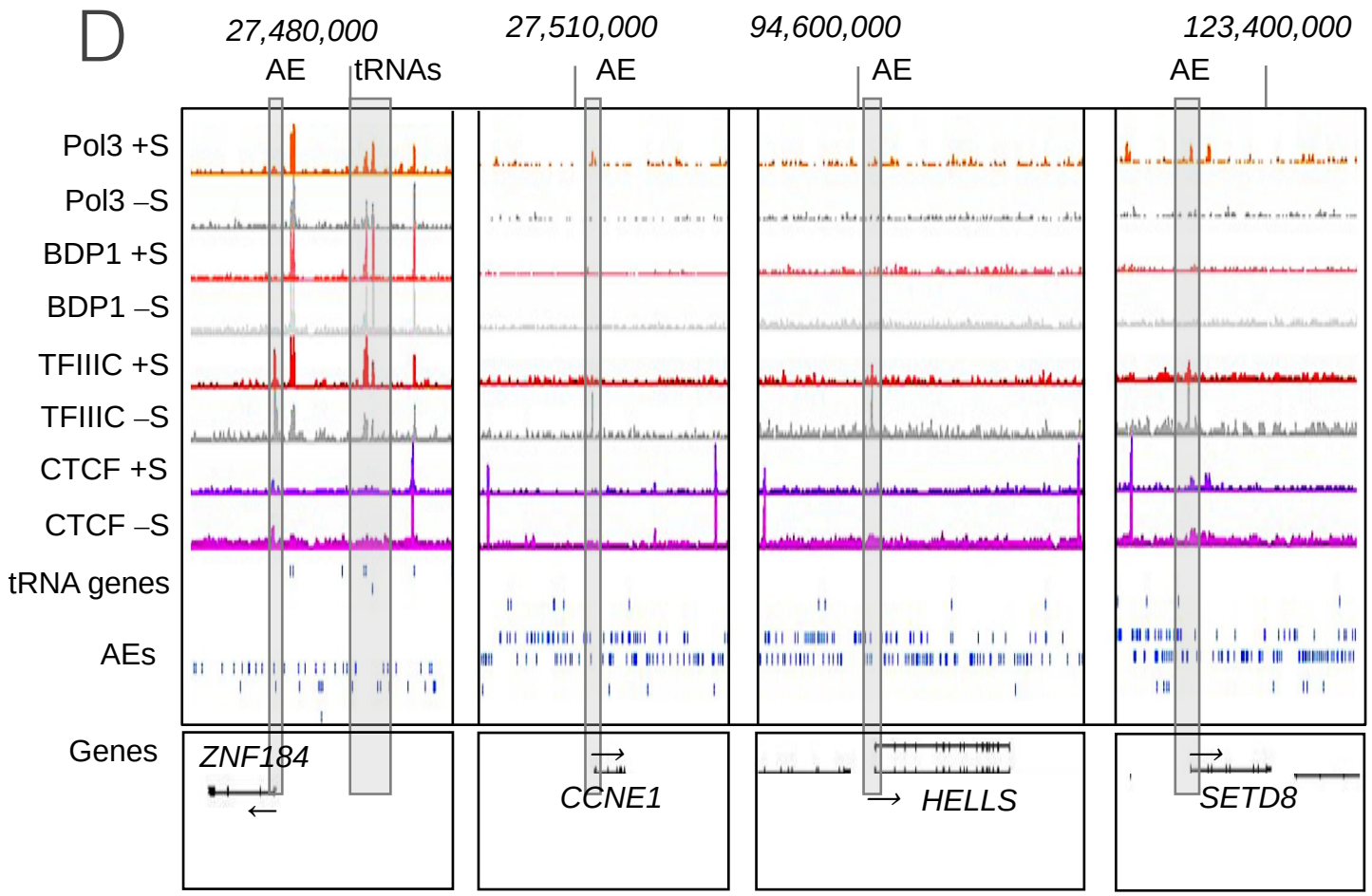
D
27,480,000
27,510,000
94,600,000
123,400,000
AE
tRNAs
Pol3 +S
Pol3 −S
BDP1 +S
BDP1 −S
TFIIIC +S
TFIIIC −S
CTCF +S
CTCF −S
tRNA genes
AEs
Genes
ZNF184
CCNE1
HELLS
SETD8

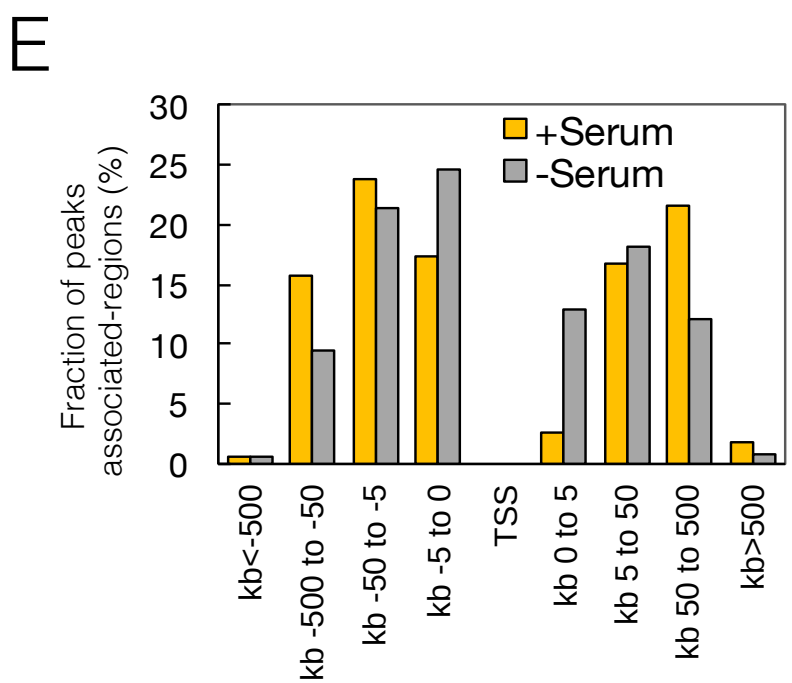
E
Fraction of peaks associated-regions (%)
+Serum
-Serum
kb<-500
kb -500 to -50
kb -50 to -5
kb -5 to 0
TSS
kb 0 to 5
kb 5 to 50
kb 50 to 500
kb>500

Figure 2

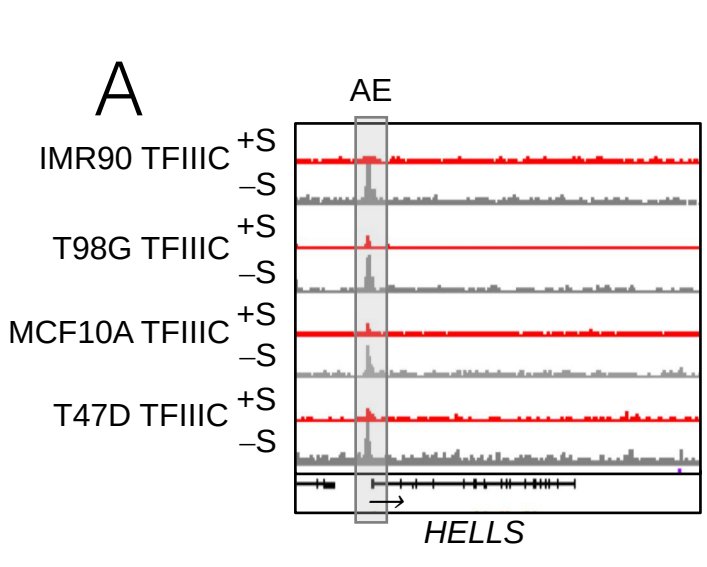
A
AE
IMR90 TFIIIC
T98G TFIIIC
MCF10A TFIIIC
T47D TFIIIC
+S
–S
HELLS

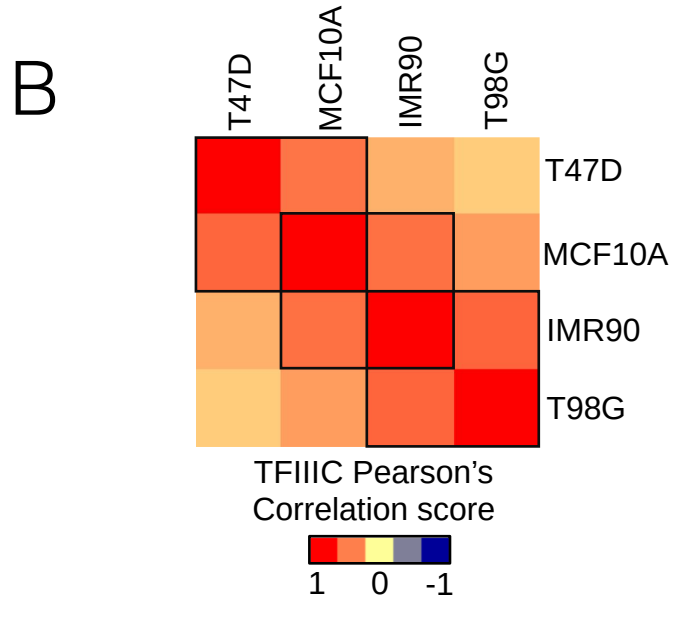
B
T47D
MCF10A
IMR90
T98G
TFIIIC Pearson's
Correlation score
1
0
-1

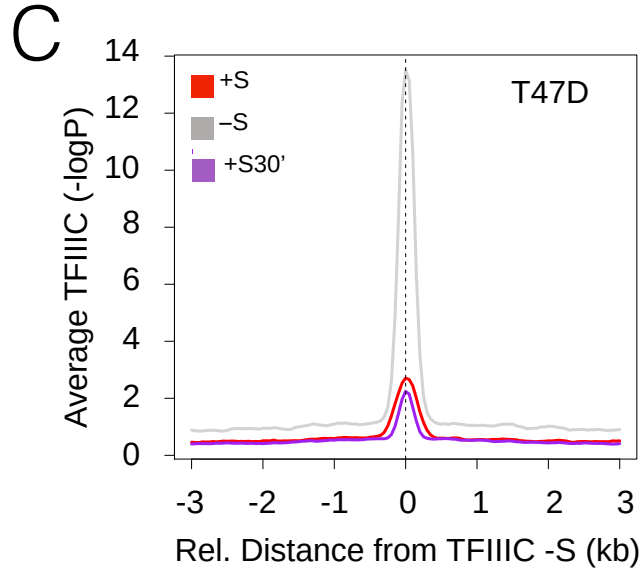
C
T47D
+S
–S
+S30'
Average TFIIIC (-logP)
Rel. Distance from TFIIIC -S (kb)

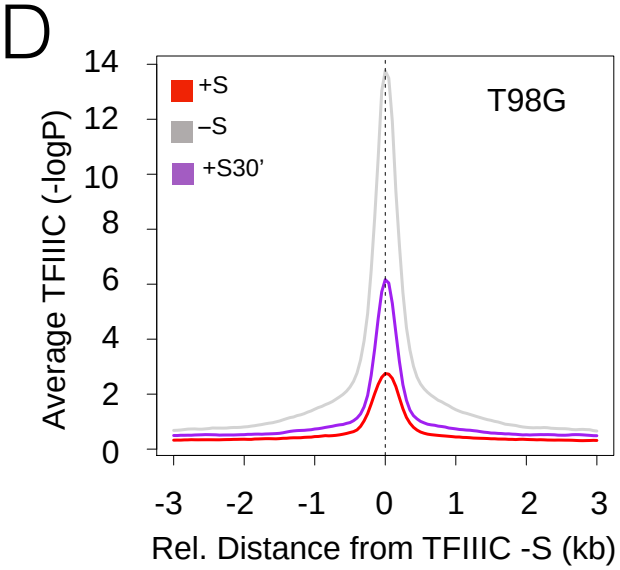
D
T98G
+S
–S
+S30'
Average TFIIIC (-logP)
Rel. Distance from TFIIIC -S (kb)

Figure 3

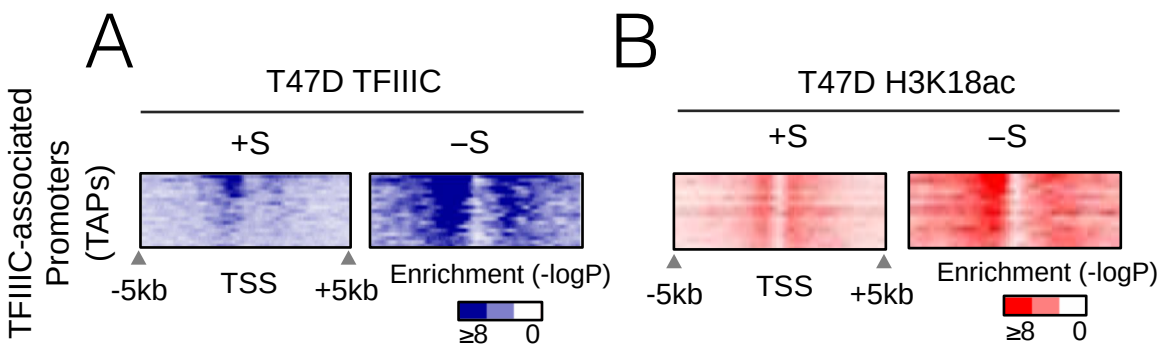
A
T47D TFIIIC
+S
–S
TFIIIC-associated Promoters (TAPs)
-5kb
TSS
+5kb
Enrichment (-logP)
≥8
0

B
T47D H3K18ac
+S
–S
-5kb
TSS
+5kb
Enrichment (-logP)
≥8
0

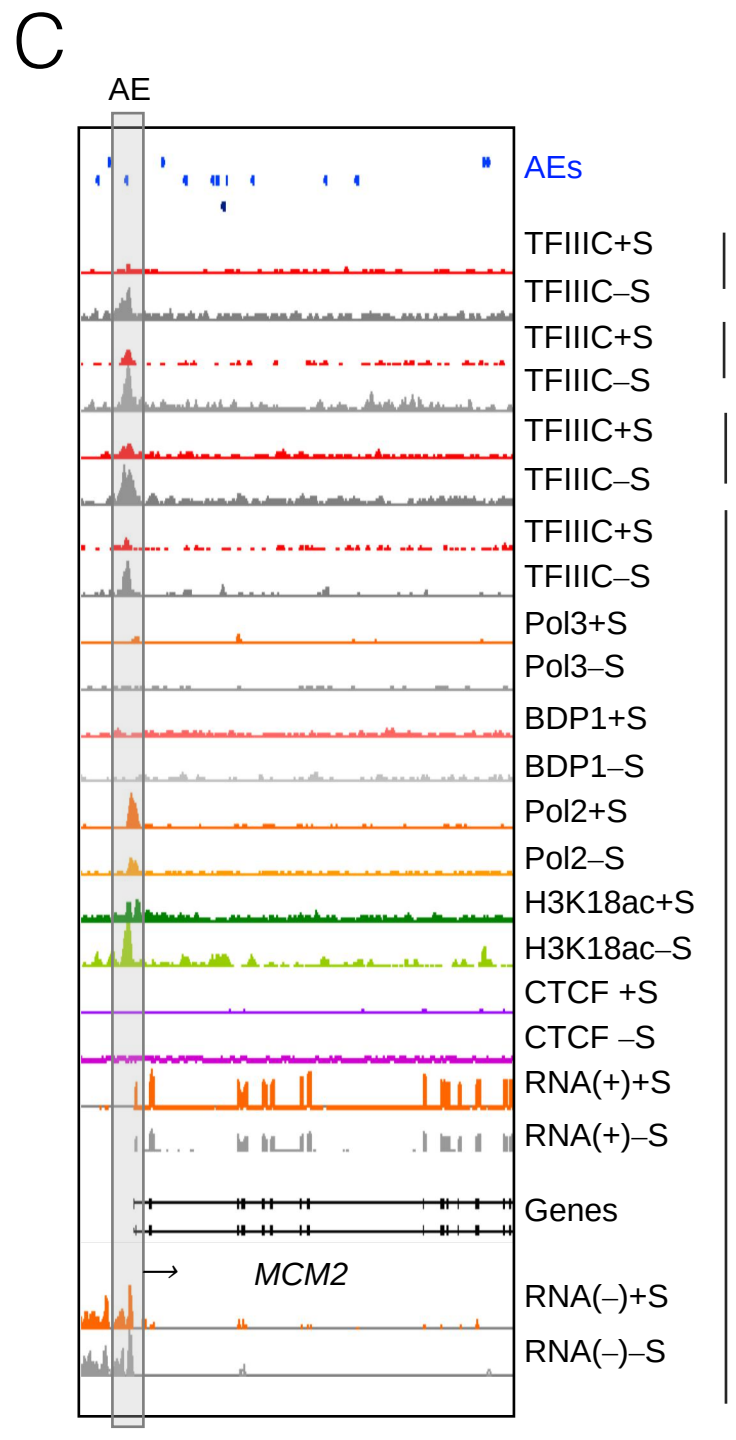
C
AE
AEs
TFIIIC+S
TFIIIC–S
TFIIIC+S
TFIIIC–S
TFIIIC+S
TFIIIC–S
TFIIIC+S
TFIIIC–S
Pol3+S
Pol3–S
BDP1+S
BDP1–S
Pol2+S
Pol2–S
H3K18ac+S
H3K18ac–S
CTCF +S
CTCF –S
RNA(+)+S
RNA(+)–S
Genes
MCM2
RNA(–)+S
RNA(–)–S
T98G
MCF10A
IMR90
T47D

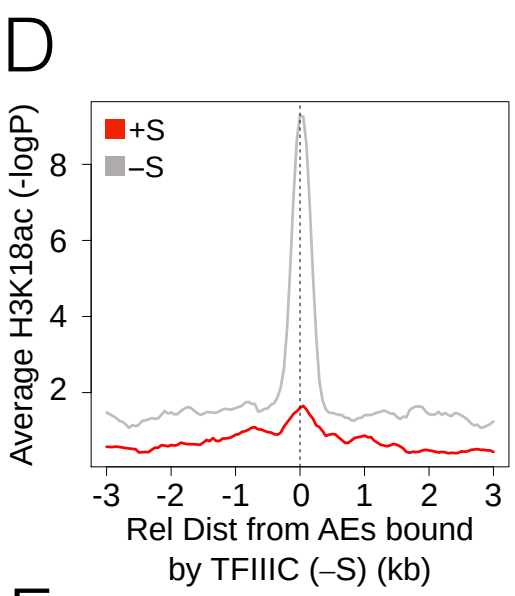
D
Average H3K18ac (-logP)
+S
–S
Rel Dist from AEs bound by TFIIIC (–S) (kb)

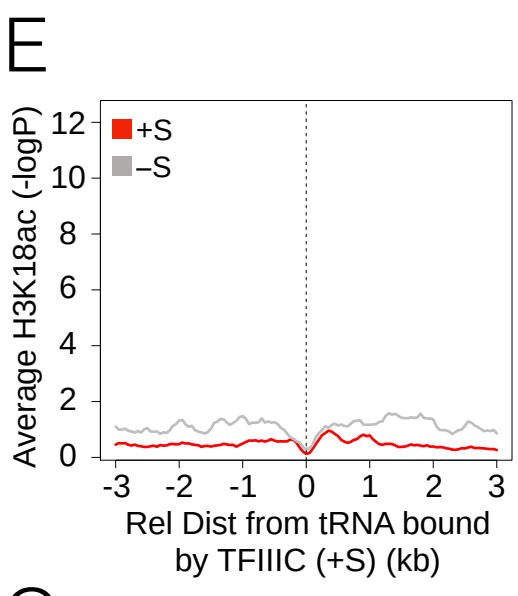
E
Average H3K18ac (-logP)
+S
–S
Rel Dist from tRNA bound by TFIIIC (+S) (kb)

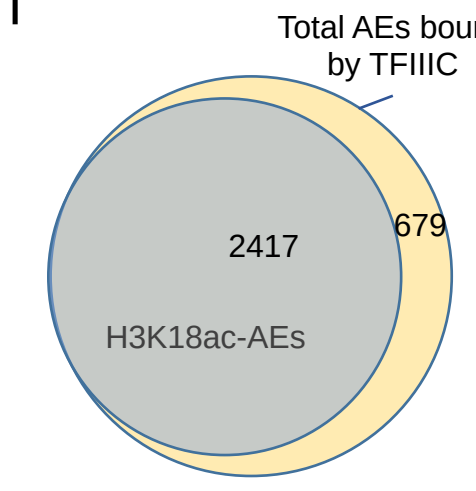
F
Total AEs bound by TFIIIC
2417
679
H3K18ac-AEs

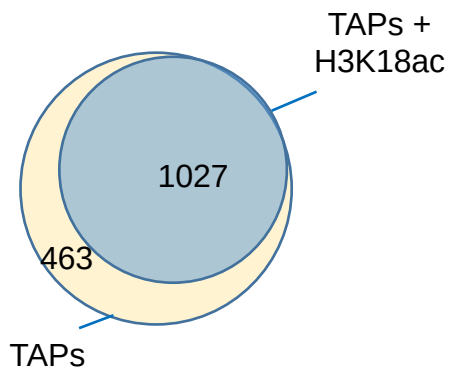
G
TAPs + H3K18ac
1027
463
TAPs

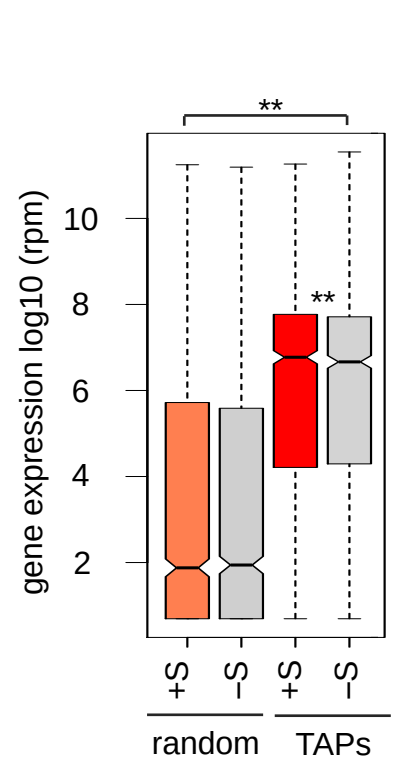
H
gene expression log10 (rpm)
**
**
+S
–S
+S
–S
random
TAPs

Figure 4

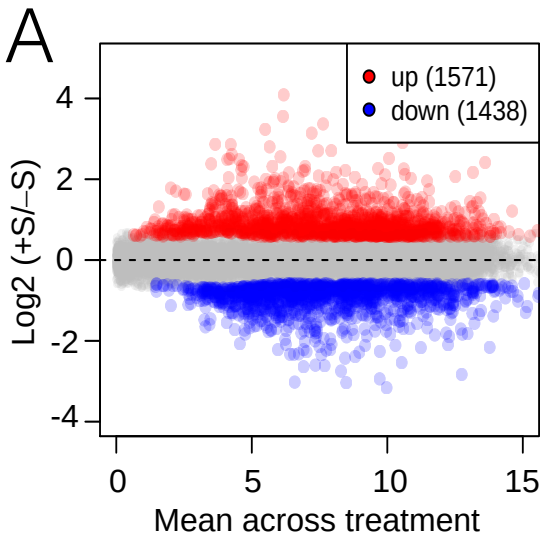
A
up (1571)
down (1438)
Log2 (+S/–S)
Mean across treatment

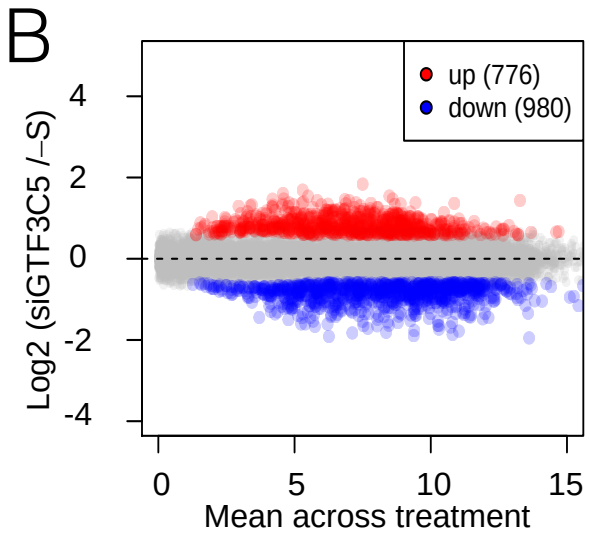
B
up (776)
down (980)
Log2 (siGTF3C5 /–S)
Mean across treatment

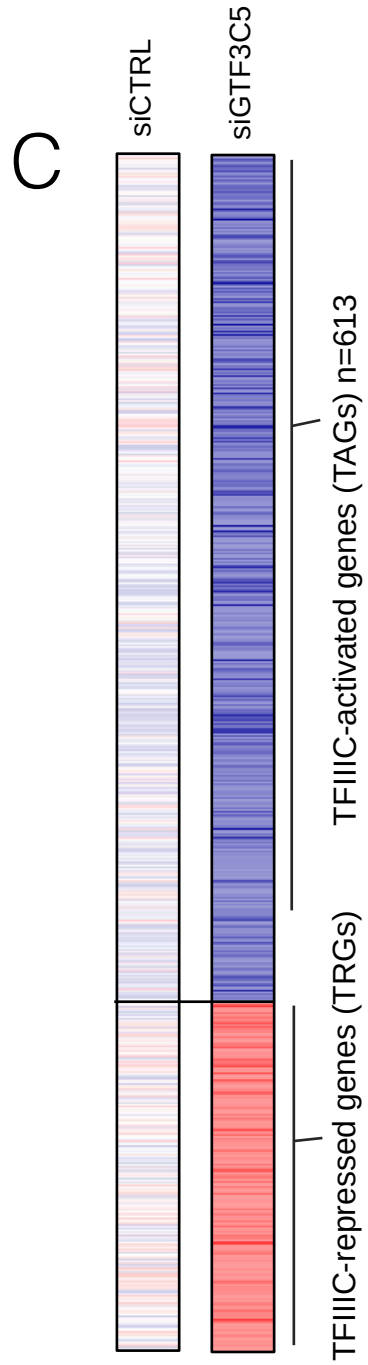
C
siCTRL
siGTF3C5
TFIIIC-activated genes (TAGs) n=613
TFIIIC-repressed genes (TRGs) n=252
Log2 ratio (compared to –S)
(normalized mRNA rpm)
2 0 -2

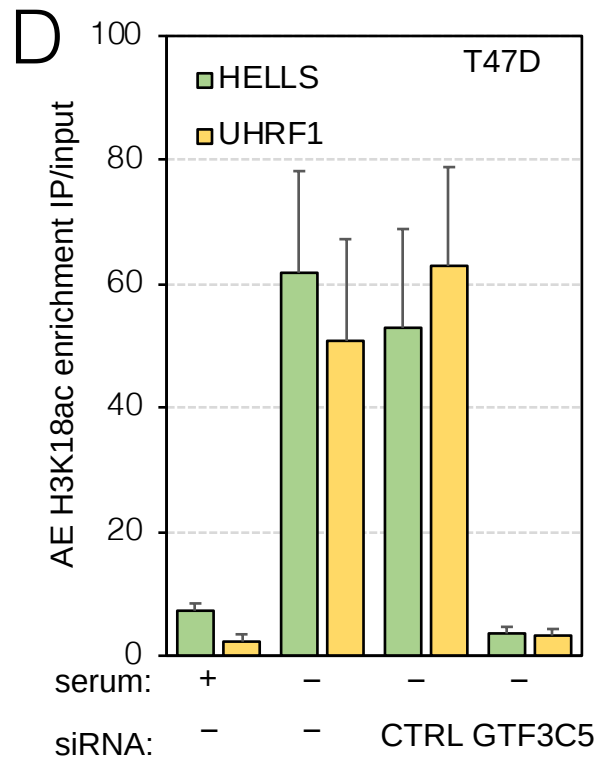
D
T47D
HELLS
UHRF1
AE H3K18ac enrichment IP/input
serum:
siRNA:
CTRL GTF3C5

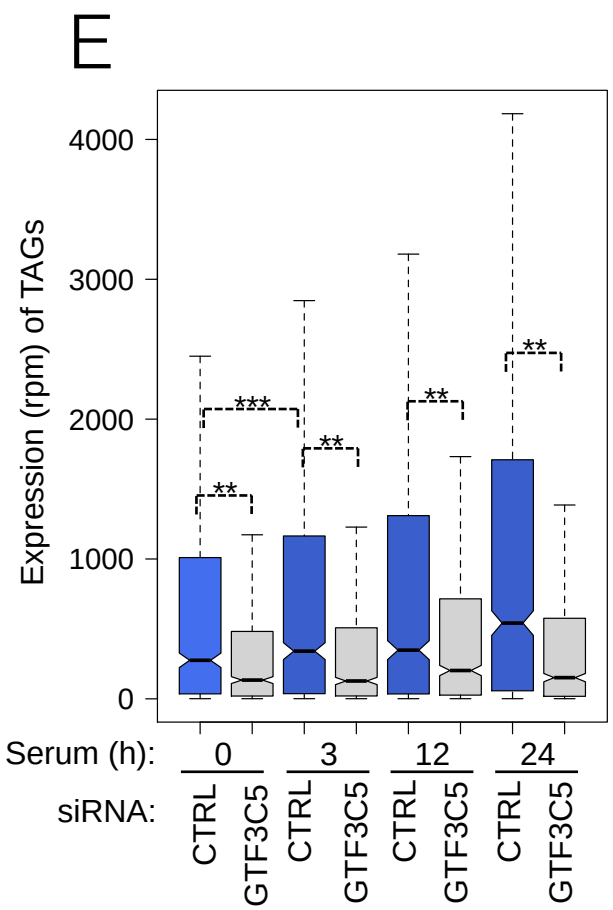
E
Expression (rpm) of TAGs
Serum (h):
siRNA:
CTRL
GTF3C5

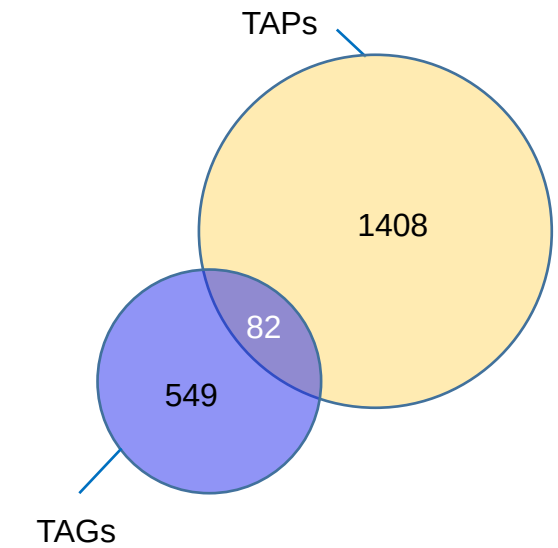
F
TAPs
1408
82
549
TAGs

Figure 5

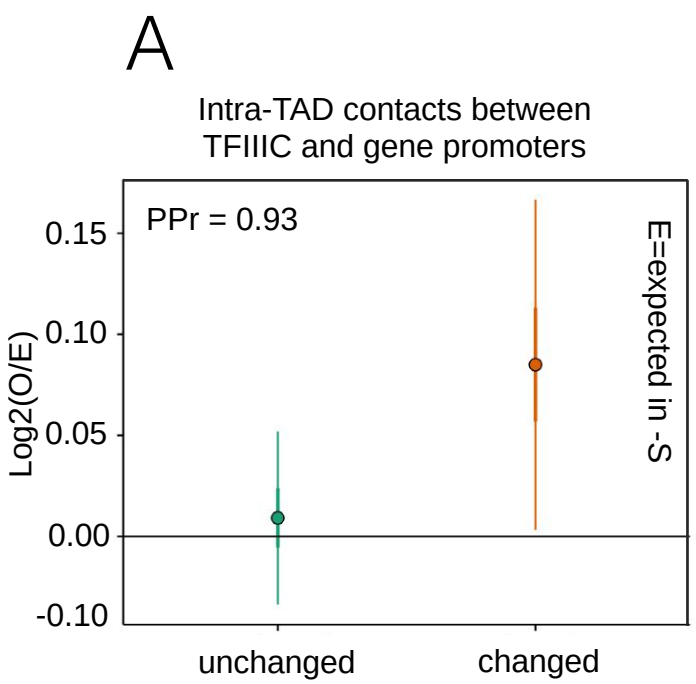
A
Intra-TAD contacts between
TFIIIC and gene promoters
PPr = 0.93
E=expected in -S
Log2(O/E)
0.15
0.10
0.05
0.00
-0.10
unchanged
changed

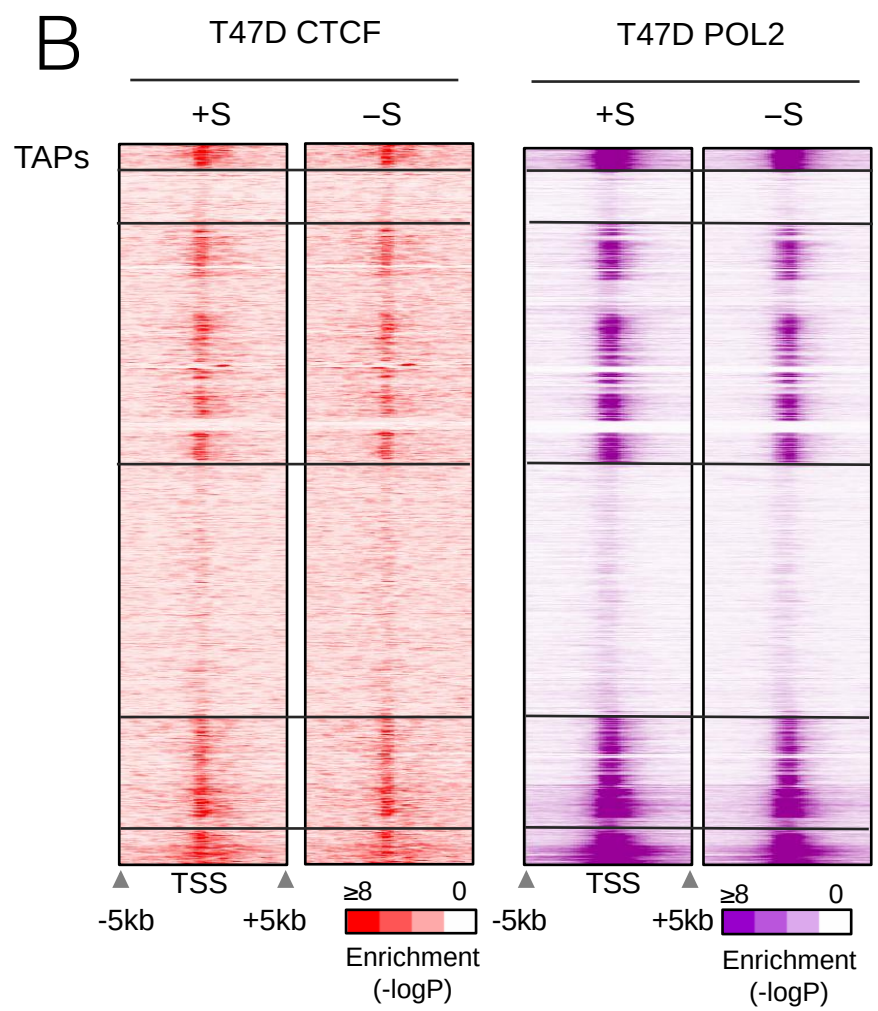
B
T47D CTCF
T47D POL2
+S
–S
+S
–S
TAPs
TSS
-5kb
+5kb
≥8
0
Enrichment
(-logP)
TSS
-5kb
+5kb
≥8
0
Enrichment
(-logP)

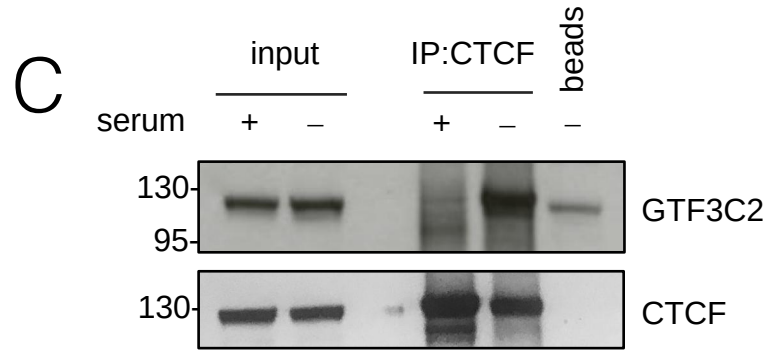
C
input
IP:CTCF
beads
serum
+
–
+
–
–
130
95
GTF3C2
130
CTCF

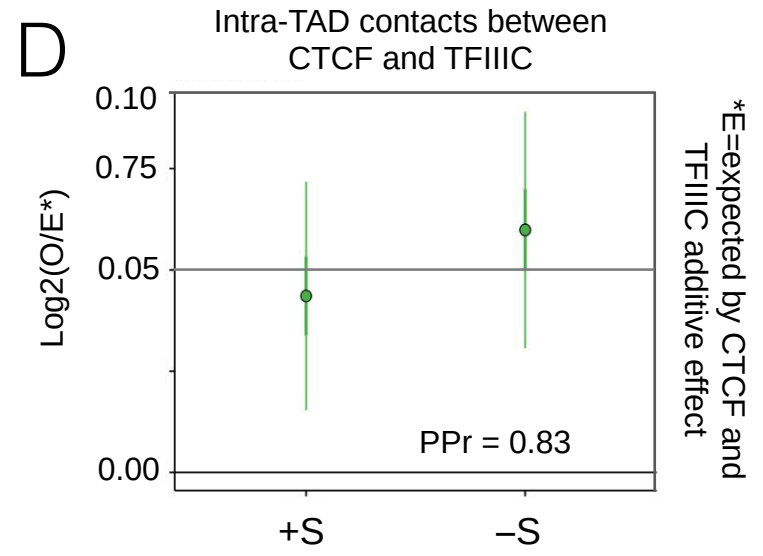
D
Intra-TAD contacts between
CTCF and TFIIIC
Log2(O/E*)
0.10
0.75
0.05
0.00
PPr = 0.83
*E=expected by CTCF and
TFIIIC additive effect
+S
–S

Figure 6

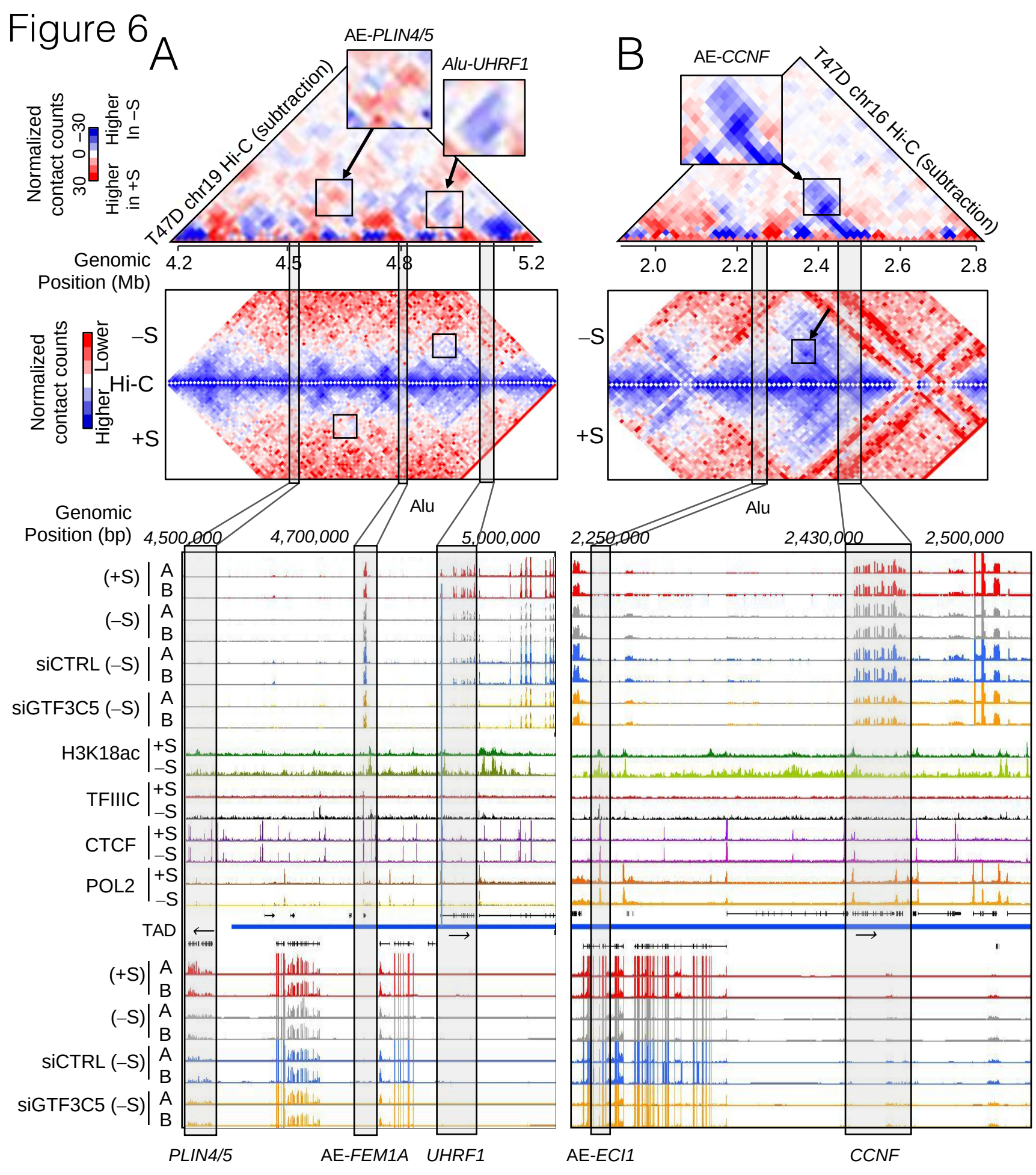
A
AE-PLIN4/5
Alu-UHRF1
T47D chr19 Hi-C (subtraction)
Normalized contact counts
30 0 −30
Higher in +S
Higher in −S
Genomic Position (Mb)
4.2
4.5
4.8
5.2
Normalized contact counts
Higher Lower
−S
Hi-C
+S
Alu
Genomic Position (bp)
4,500,000
4,700,000
5,000,000
(+S) A B
(−S) A B
siCTRL (−S) A B
siGTF3C5 (−S) A B
H3K18ac +S −S
TFIIIC +S −S
CTCF +S −S
POL2 +S −S
TAD
(+S) A B
(−S) A B
siCTRL (−S) A B
siGTF3C5 (−S) A B
PLIN4/5
AE-FEM1A
UHRF1
B
AE-CCNF
T47D chr16 Hi-C (subtraction)
2.0
2.2
2.4
2.6
2.8
−S
+S
Alu
2,250,000
2,430,000
2,500,000
AE-ECI1
CCNF

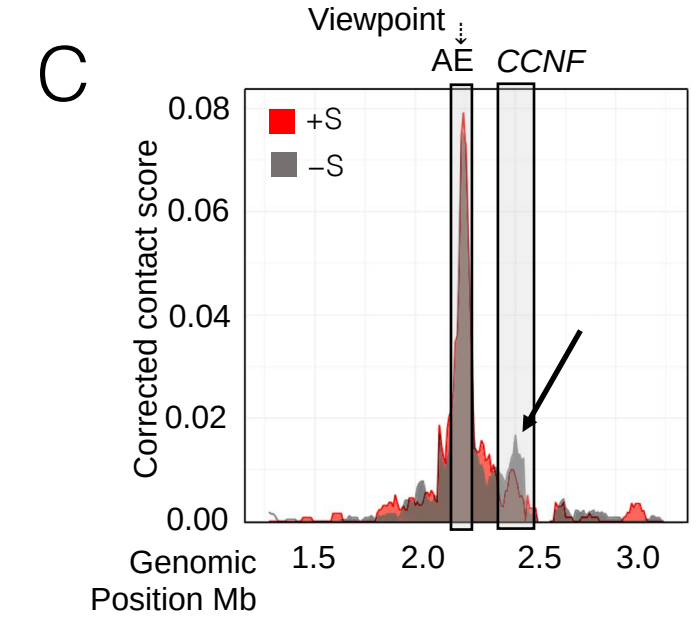
C
Viewpoint
AE
CCNF
+S
−S
Corrected contact score
0.08
0.06
0.04
0.02
0.00
Genomic Position Mb
1.5
2.0
2.5
3.0

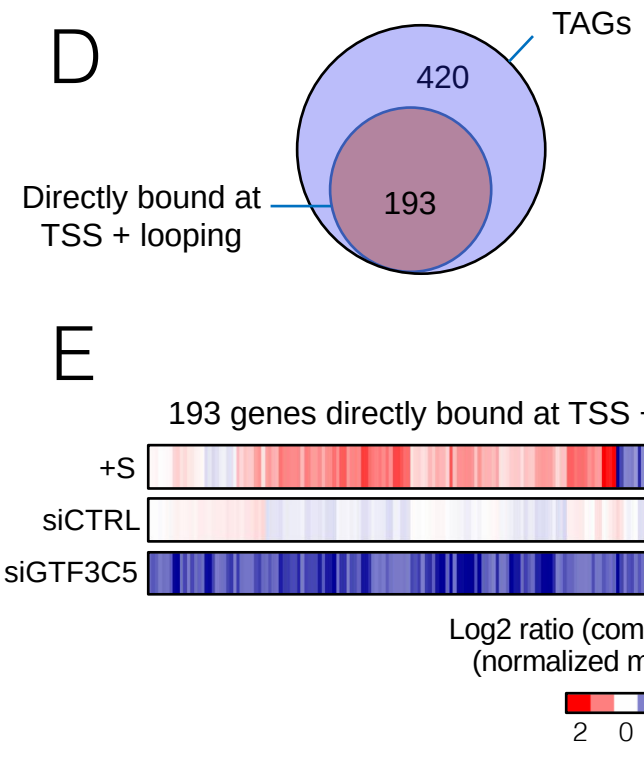
D
TAGs
420
193
Directly bound at TSS + looping
E
193 genes directly bound at TSS + looping
+S
siCTRL
siGTF3C5
Log2 ratio (compared to −S) (normalized mRNA rpm)
2 0 -2
F
Number of significant CTCF binding events Within a 10 kb window around TSS
p=0.00667
random
looped
0
5
10
15
20

Figure 7

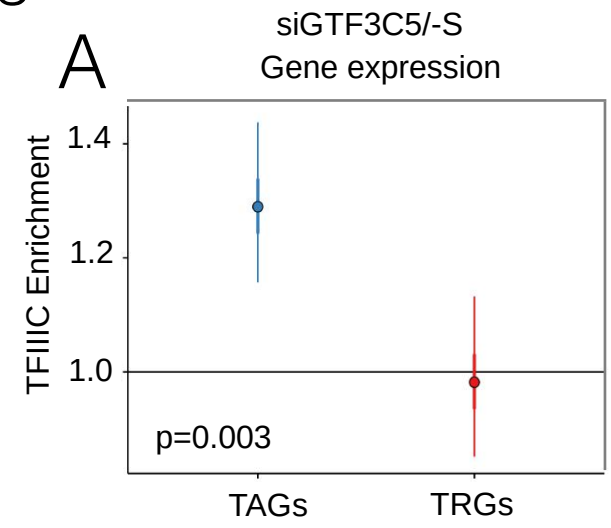
A
siGTF3C5/-S
Gene expression
TFIIIC Enrichment
1.4
1.2
1.0
p=0.003
TAGs
TRGs

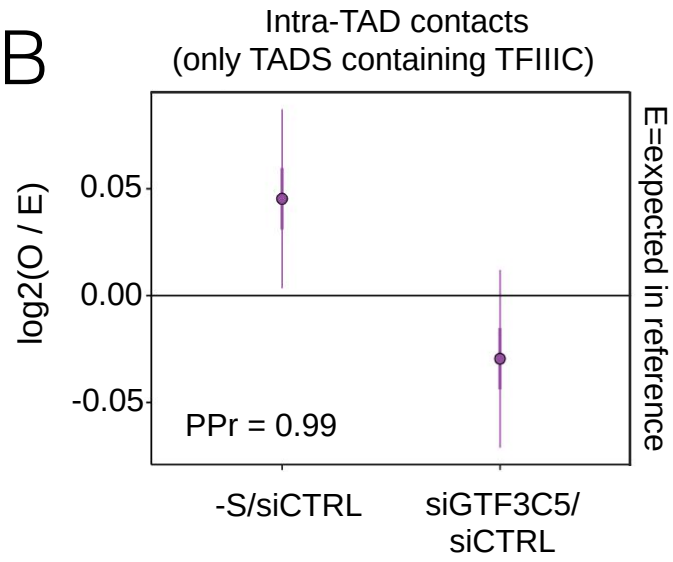
B
Intra-TAD contacts
(only TADS containing TFIIIC)
log2(O / E)
0.05
0.00
-0.05
PPr = 0.99
E=expected in reference
-S/siCTRL
siGTF3C5/
siCTRL

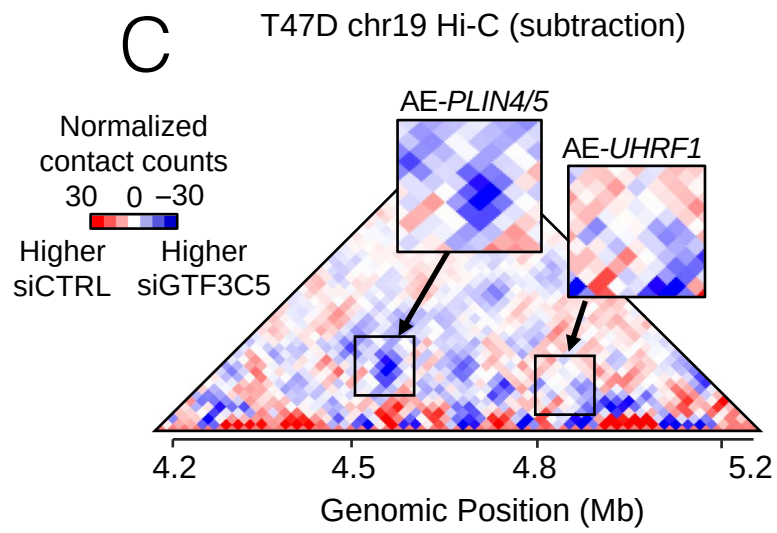
C
T47D chr19 Hi-C (subtraction)
Normalized
contact counts
30 0 –30
Higher
siCTRL
Higher
siGTF3C5
AE-PLIN4/5
AE-UHRF1
4.2
4.5
4.8
5.2
Genomic Position (Mb)

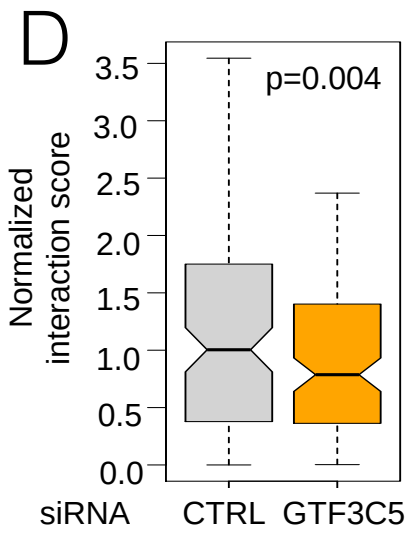
D
Normalized
interaction score
3.5
3.0
2.5
2.0
1.5
1.0
0.5
0.0
p=0.004
siRNA
CTRL
GTF3C5

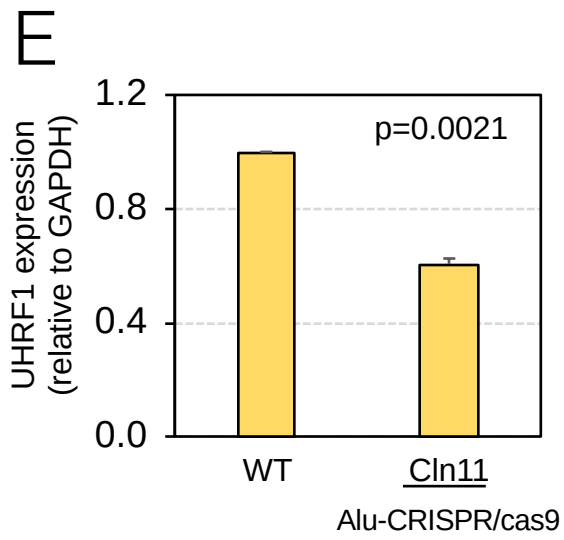
E
UHRF1 expression
(relative to GAPDH)
1.2
0.8
0.4
0.0
p=0.0021
WT
Cln11
Alu-CRISPR/cas9

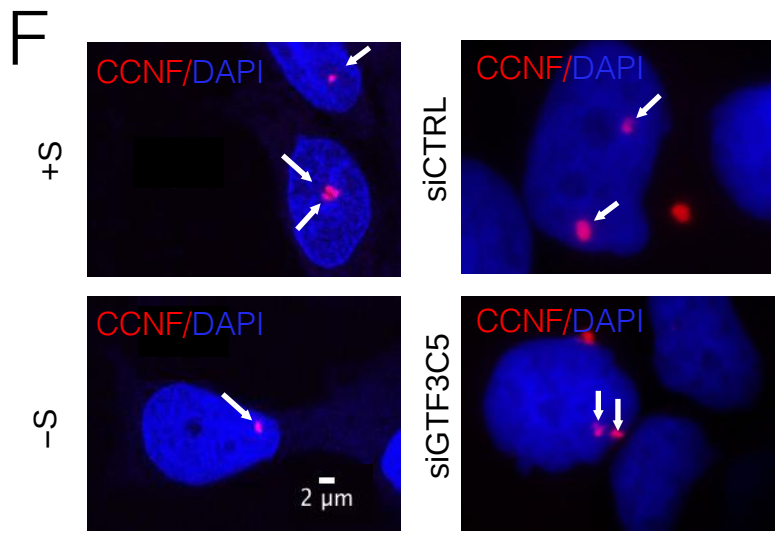
F
+S
–S
siCTRL
siGTF3C5
CCNF/DAPI
2 µm

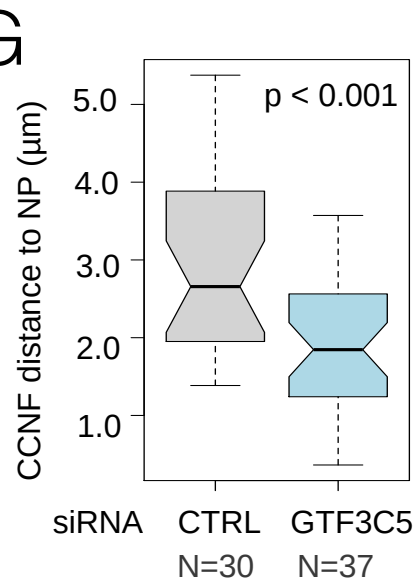
G
CCNF distance to NP (µm)
5.0
4.0
3.0
2.0
1.0
p < 0.001
siRNA
CTRL
GTF3C5
N=30
N=37

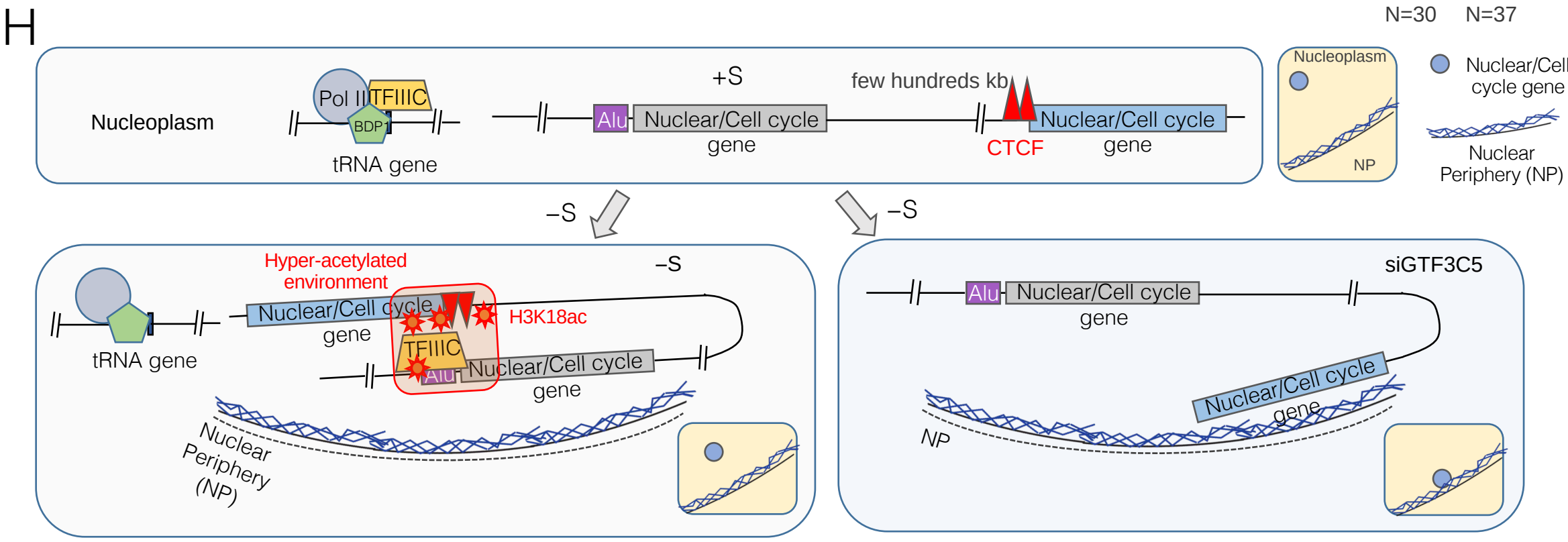
H
Nucleoplasm
Pol II
TFIIIC
BDP1
tRNA gene
+S
Alu
Nuclear/Cell cycle
gene
few hundreds kb
CTCF
Nucleoplasm
NP
Nuclear/Cell
cycle gene
Nuclear
Periphery (NP)
–S
–S
Hyper-acetylated
environment
H3K18ac
TFIIIC
siGTF3C5
Nuclear
Periphery
(NP)

Supp. Figure 1

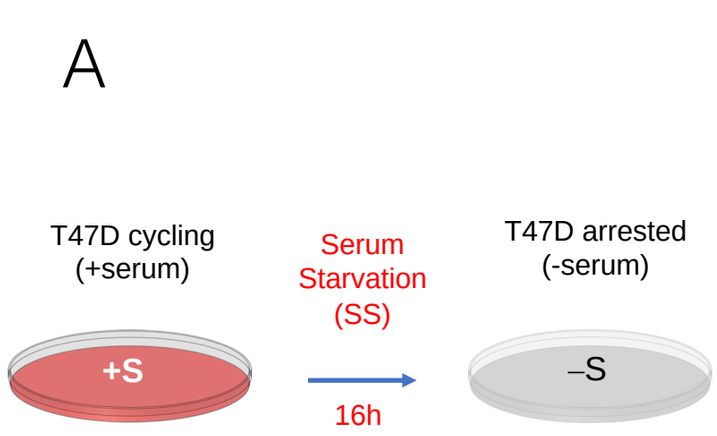

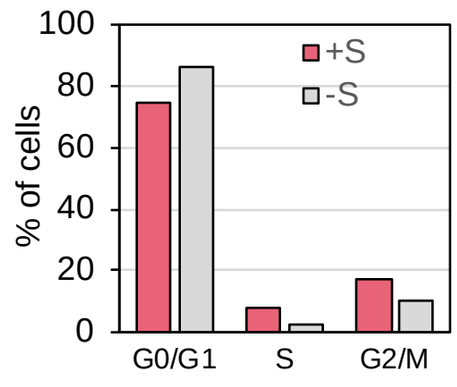

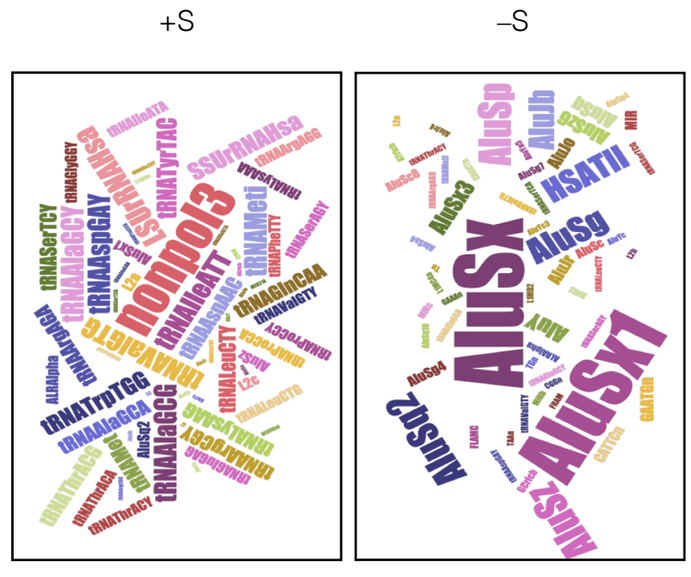

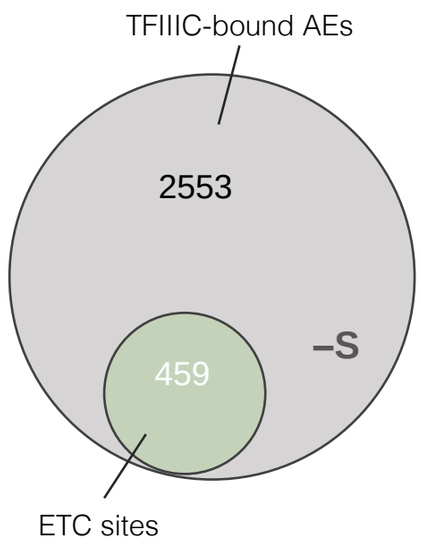

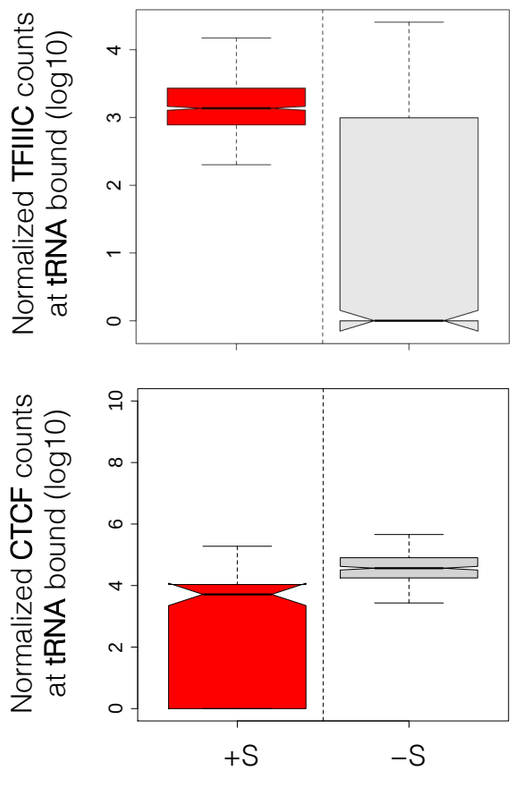

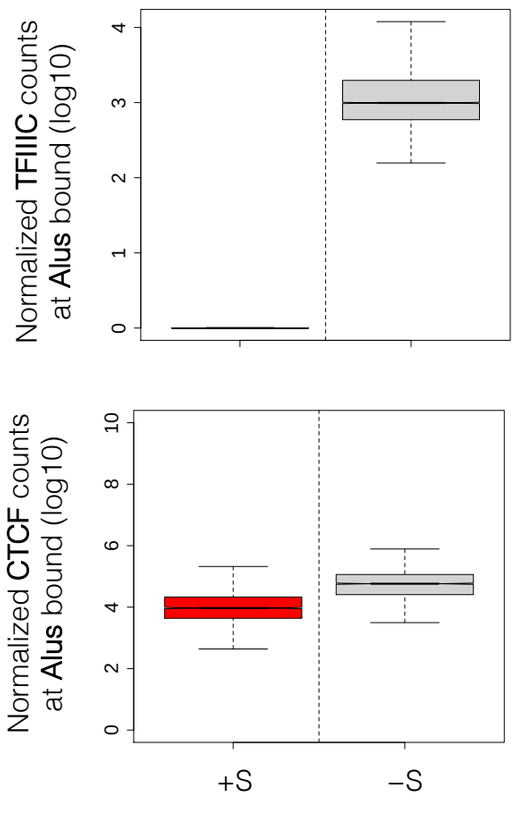

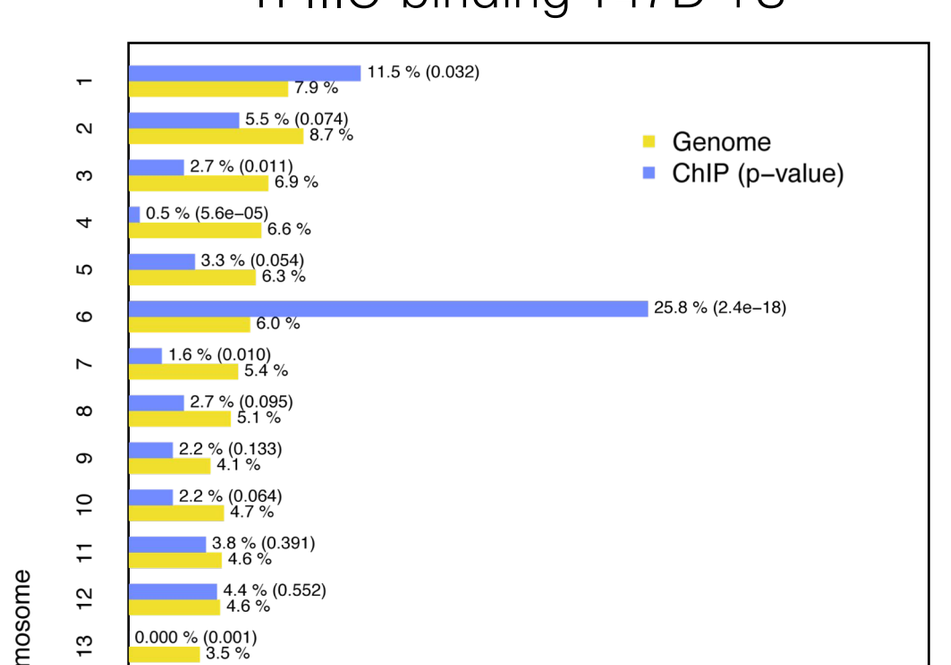

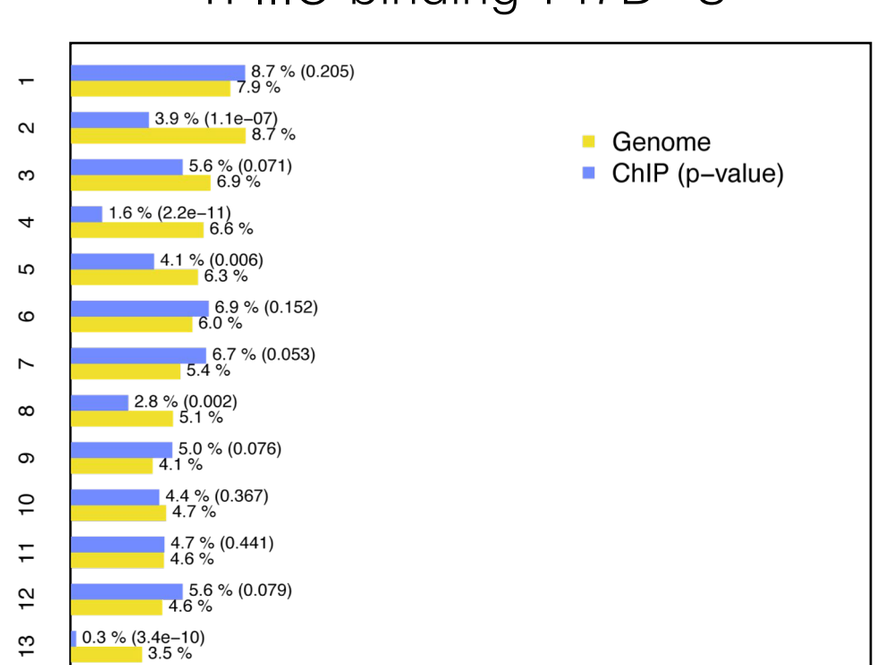

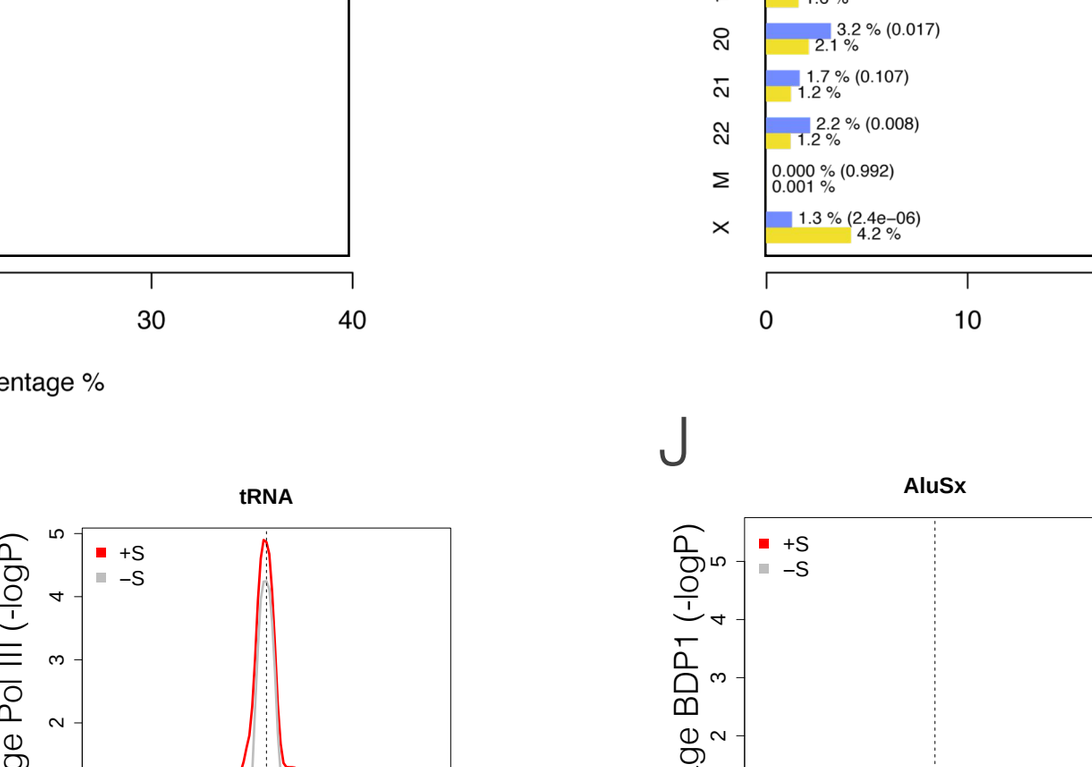

Supp. Figure 2

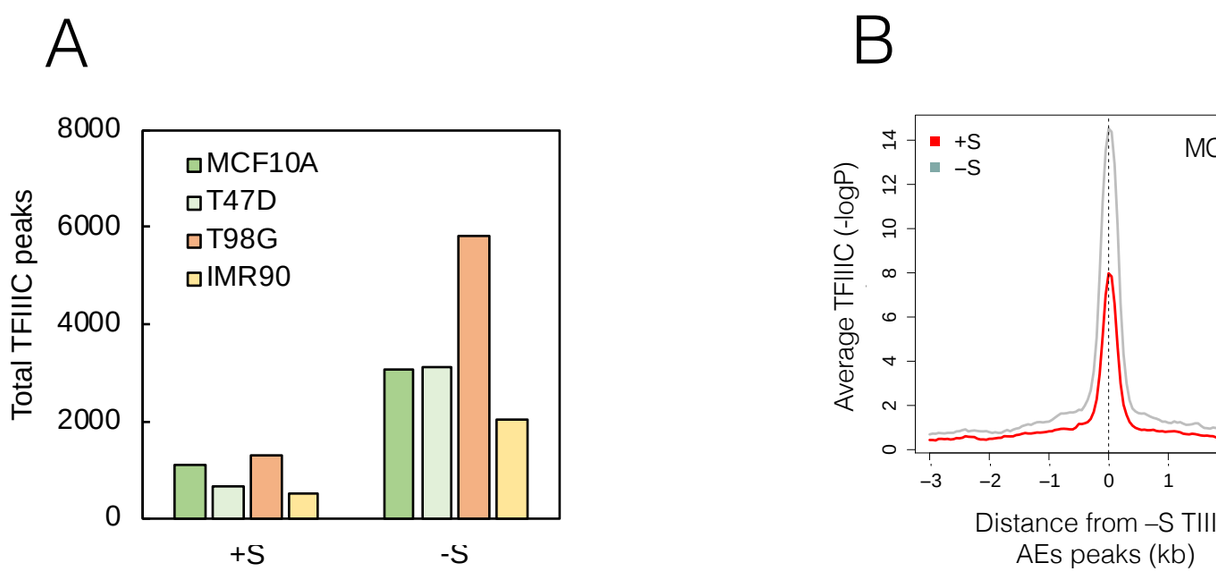

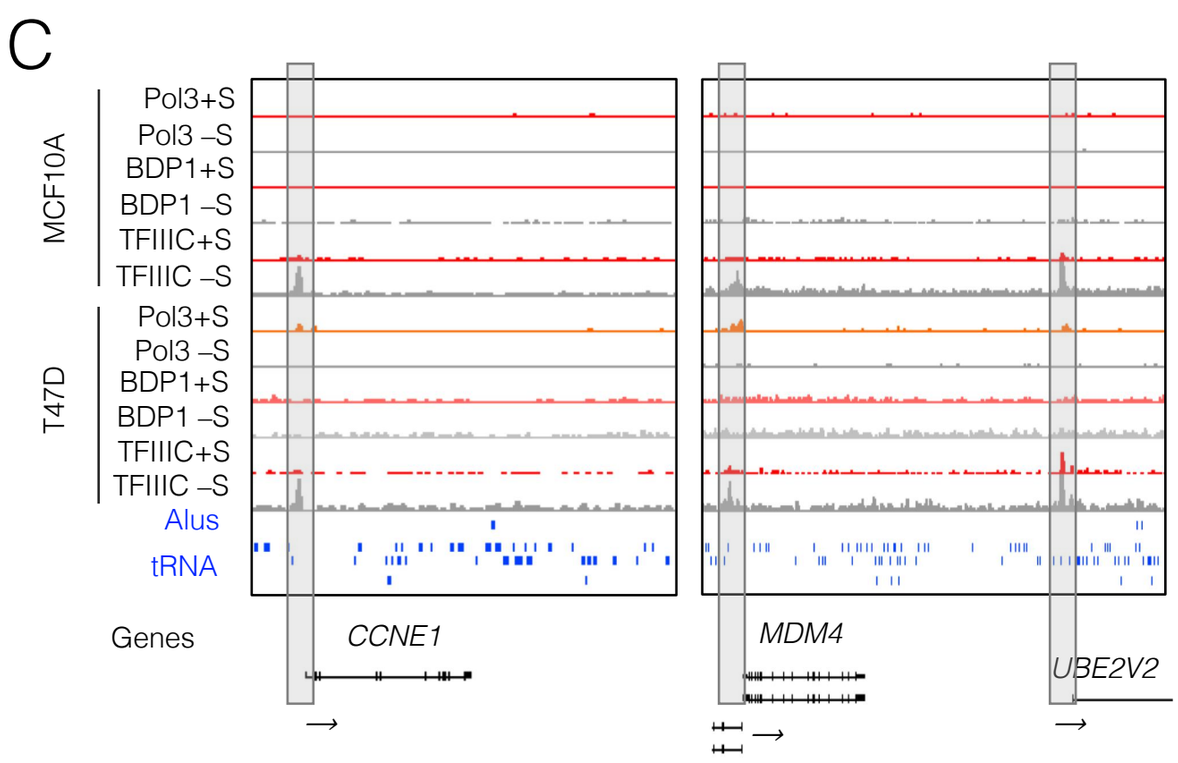

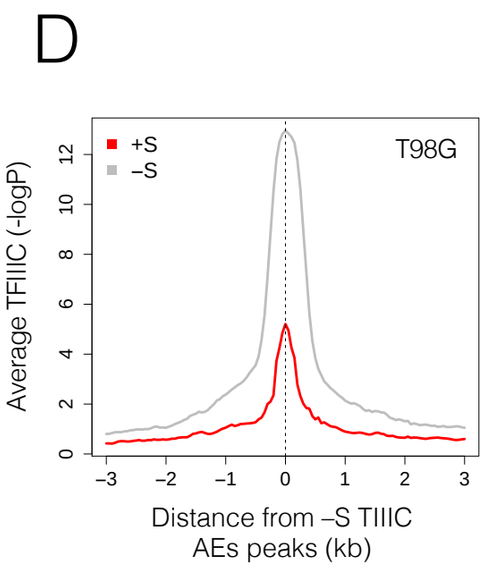

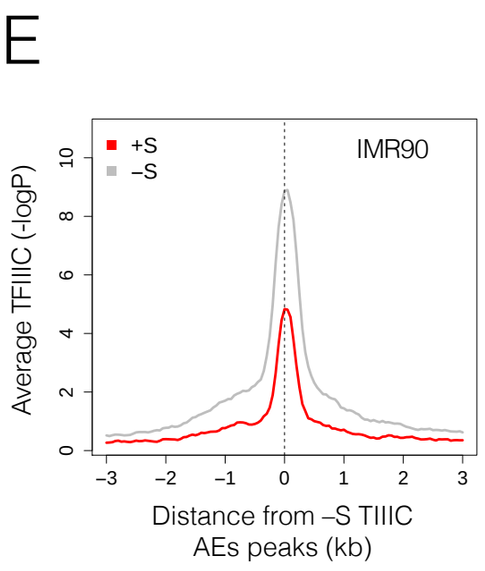

Supp. Figure 3

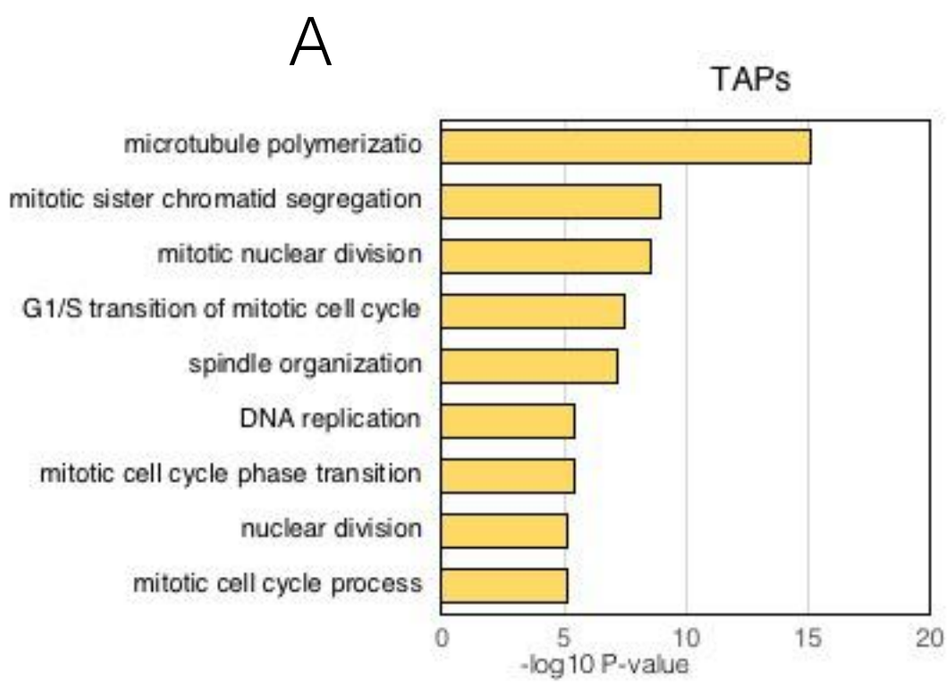

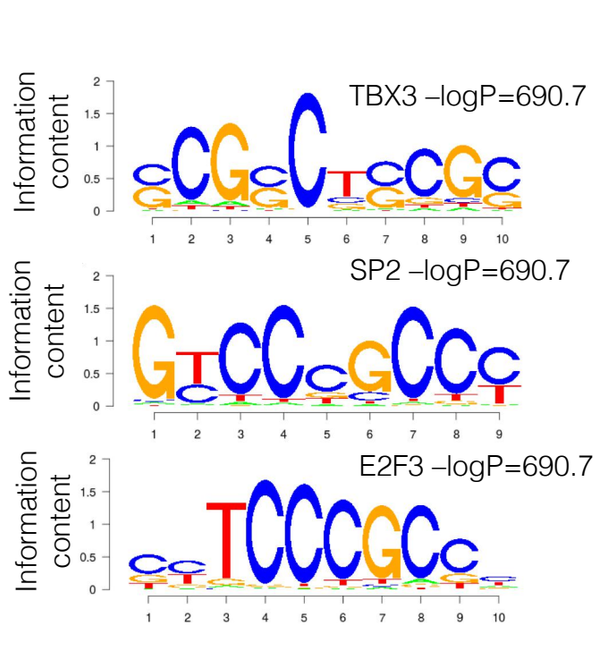

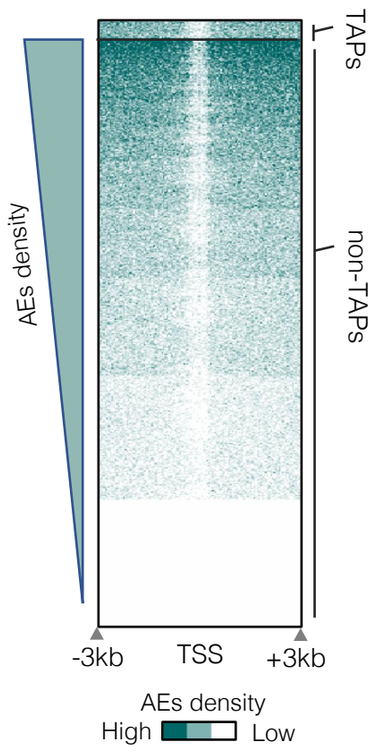

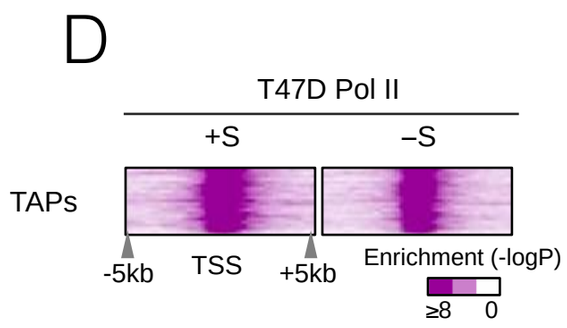

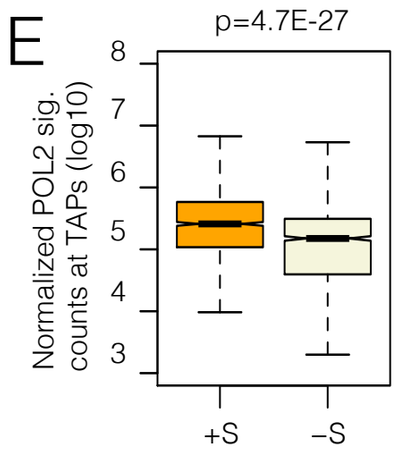

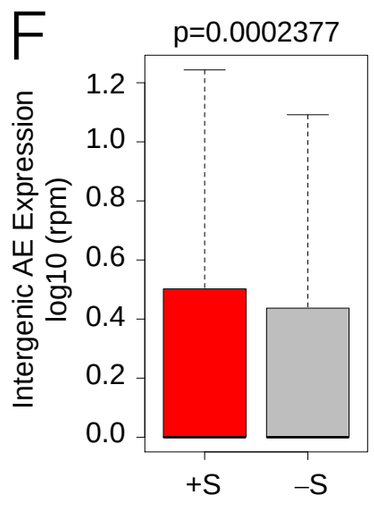

Supp. Figure 4

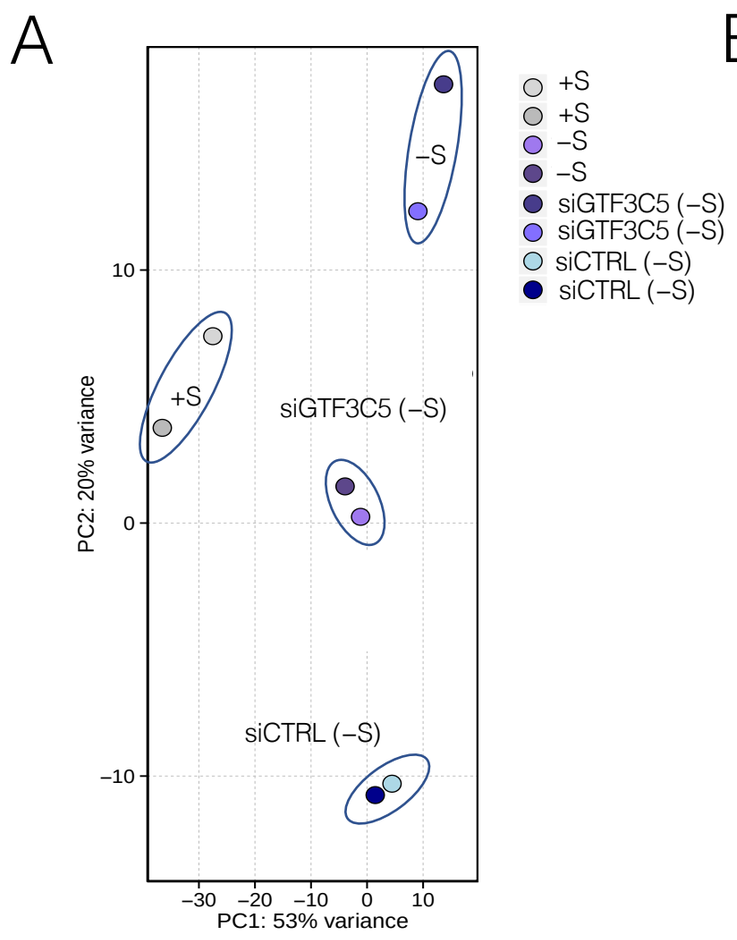

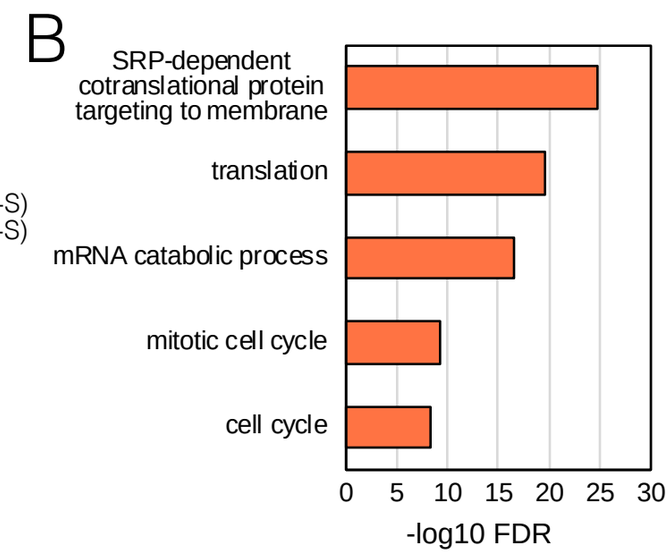

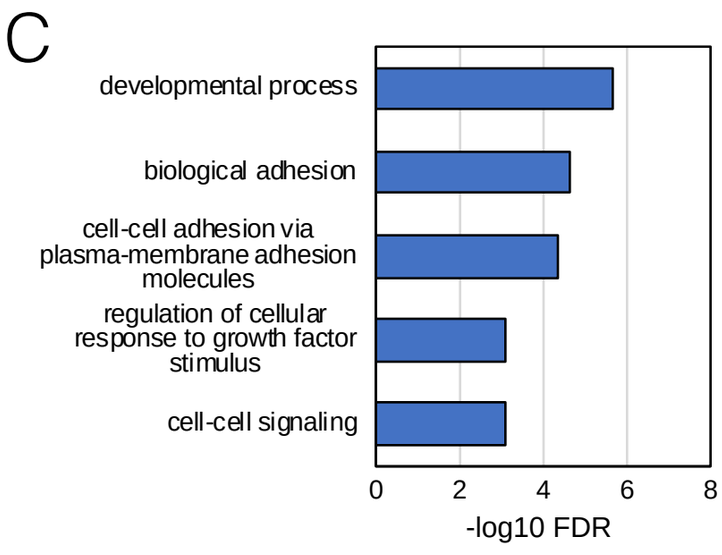

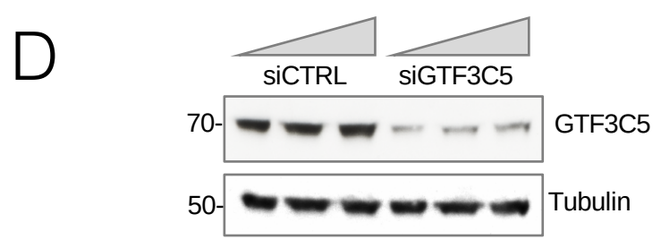

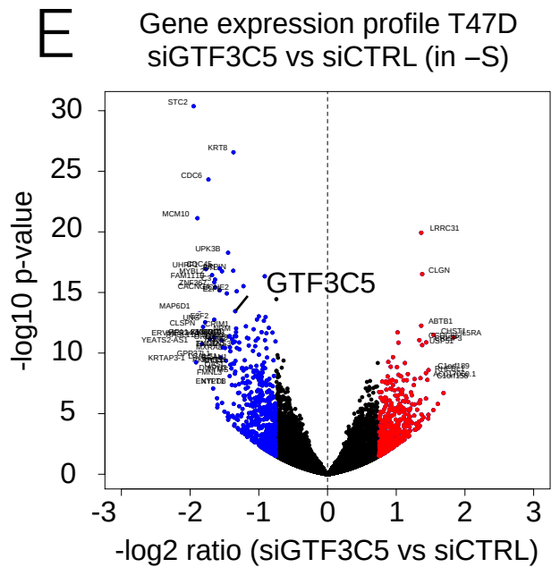

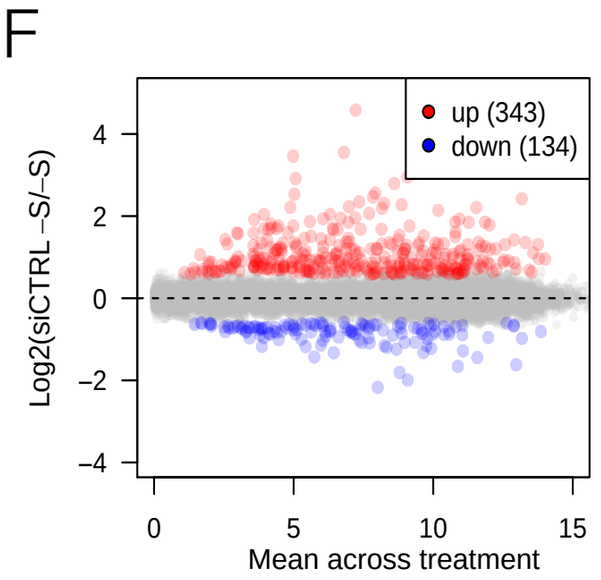

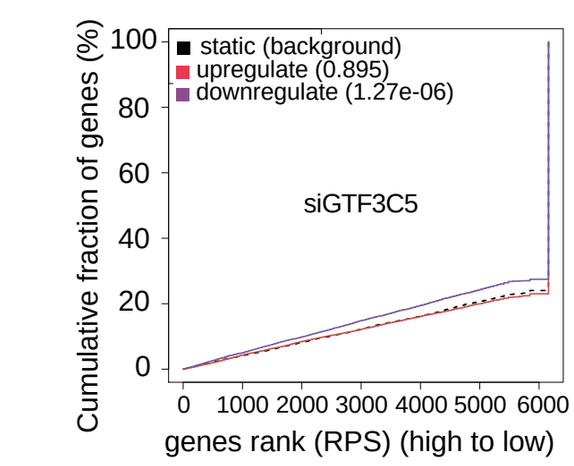

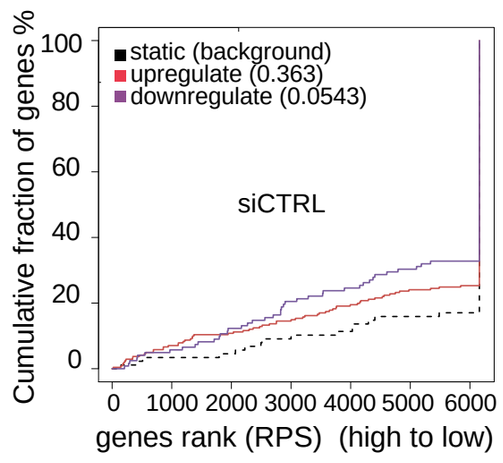

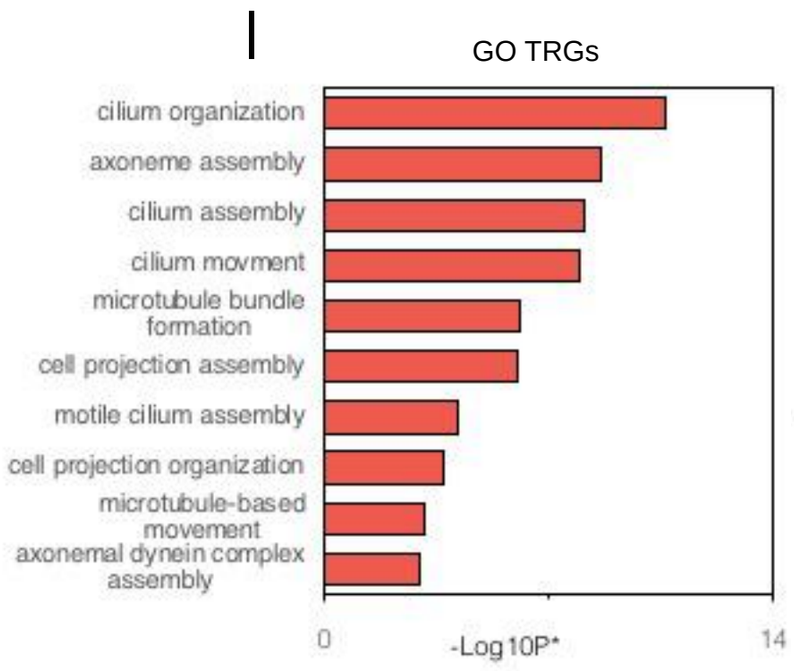

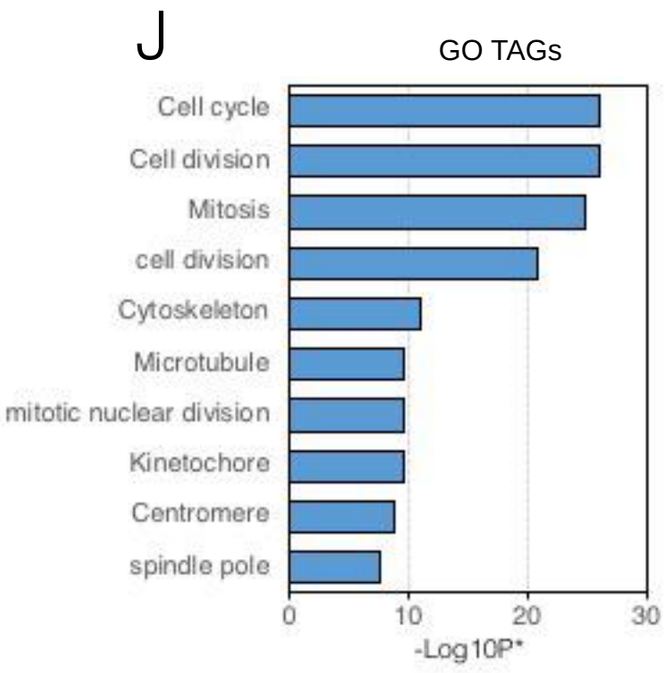

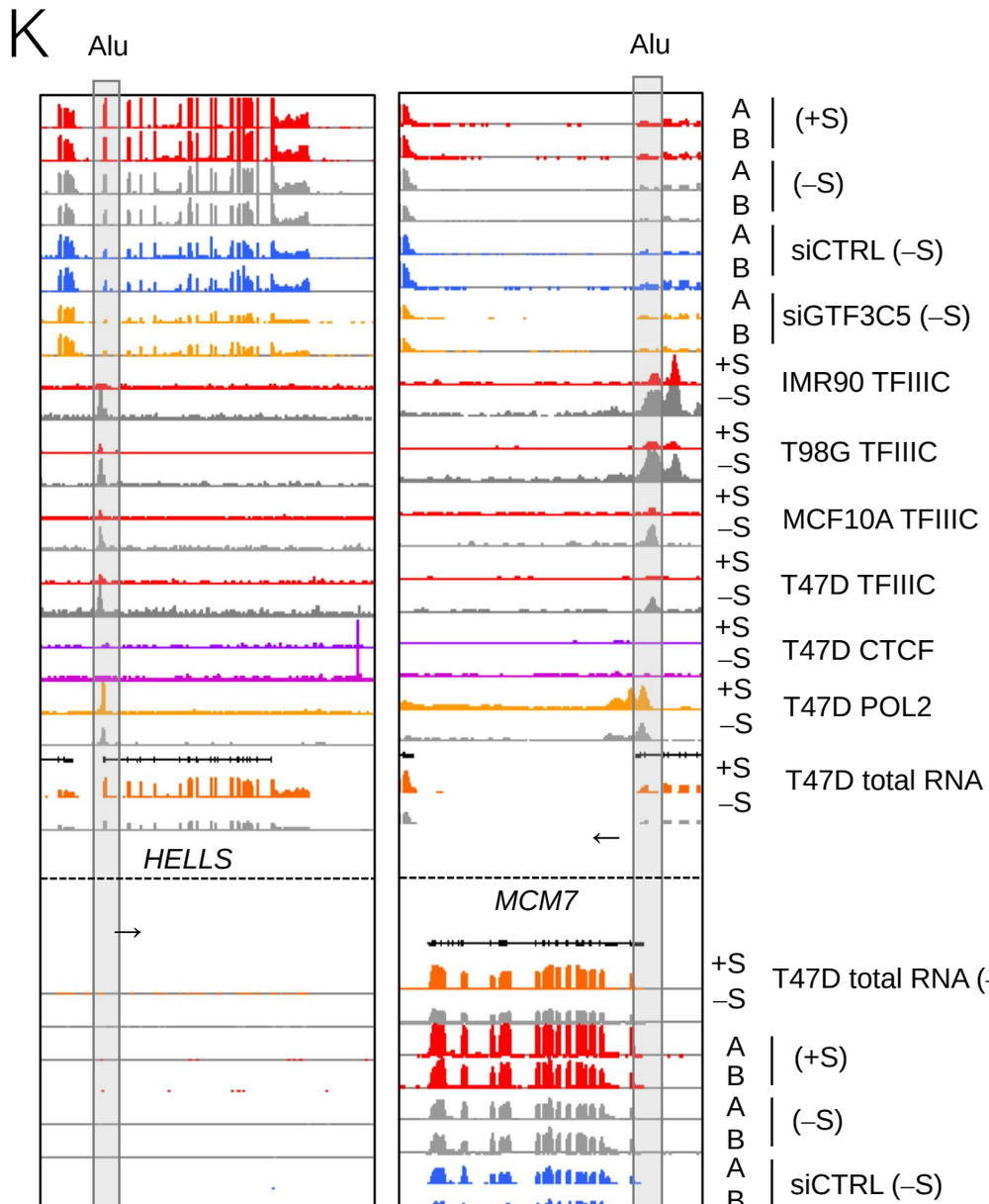

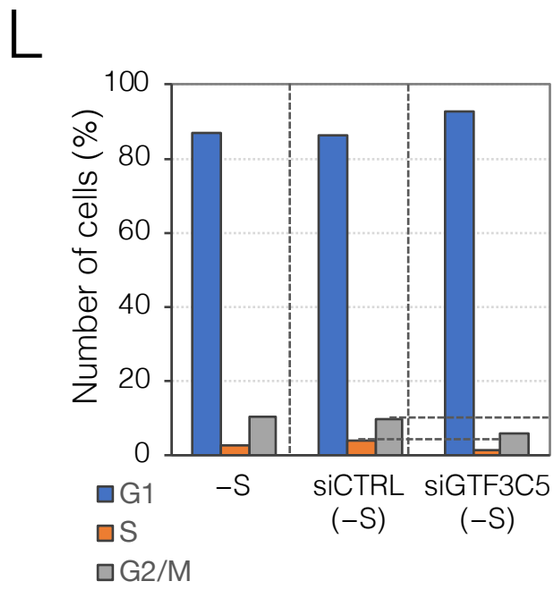

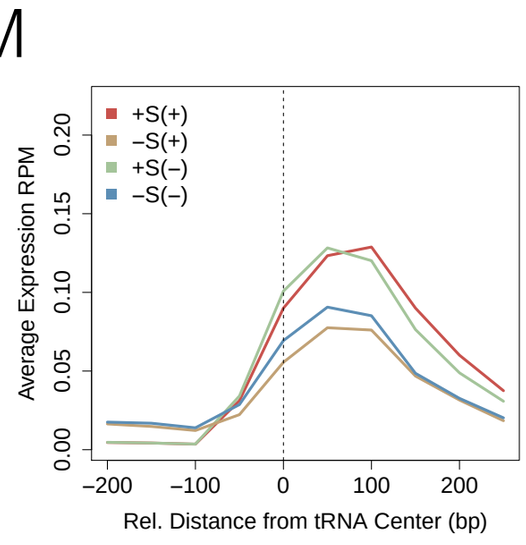

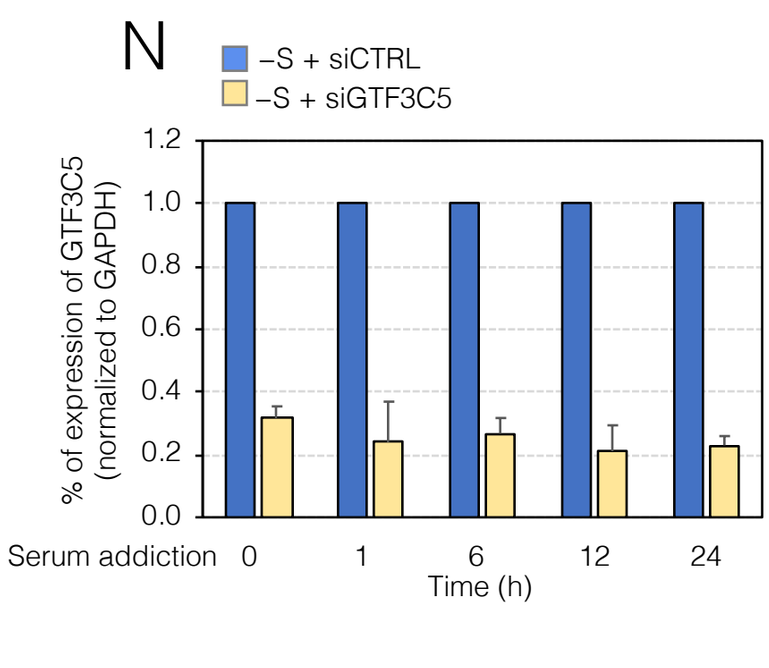

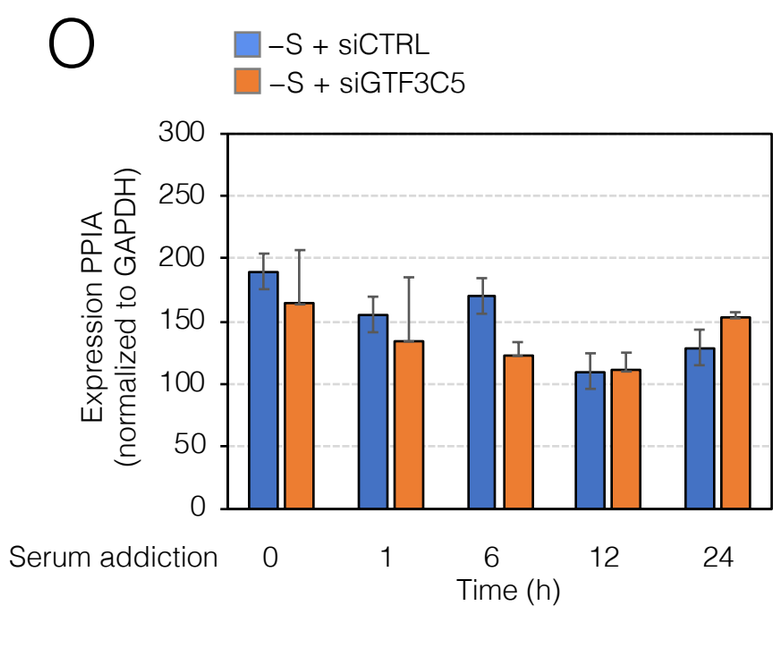

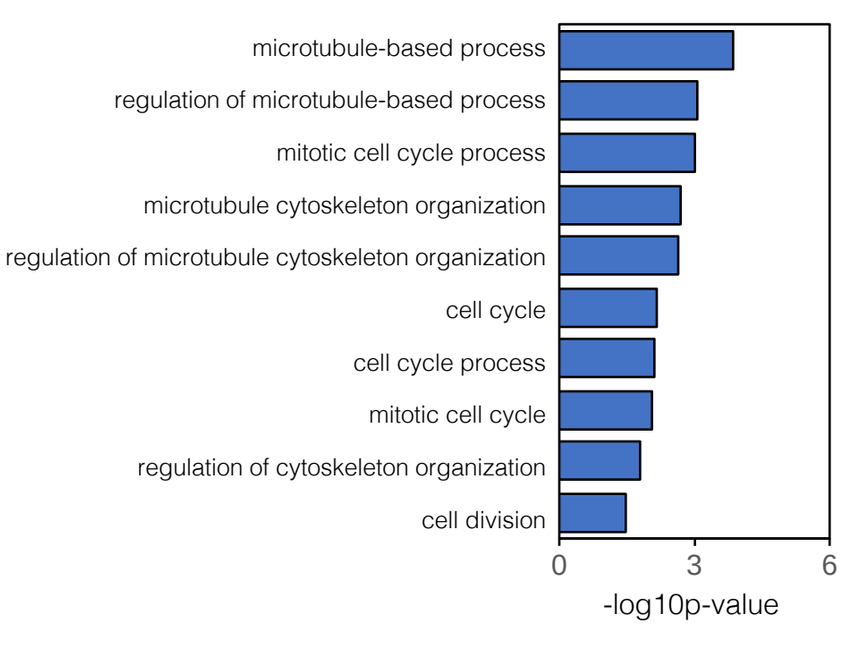

Supp. Figure 5

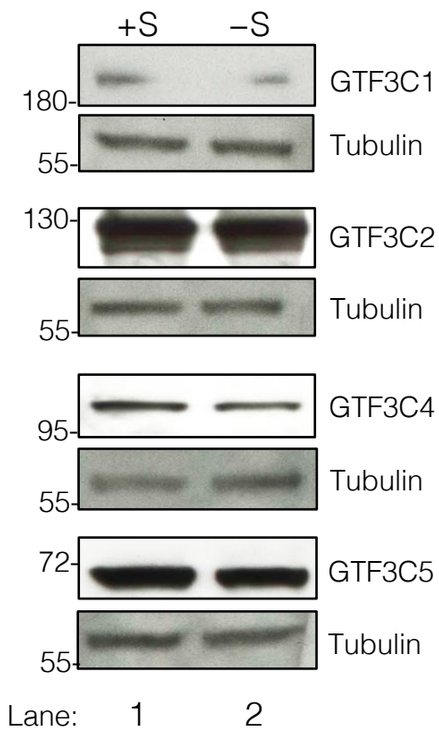

Supp. Figure 6

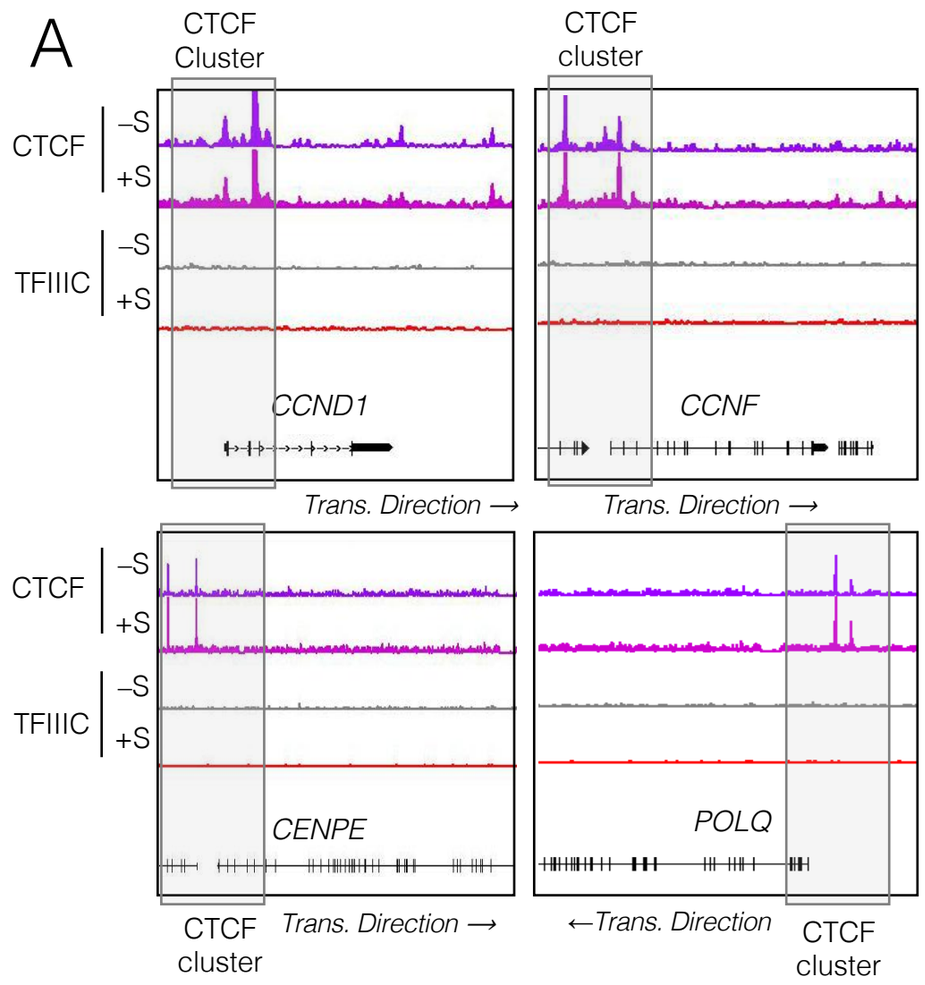

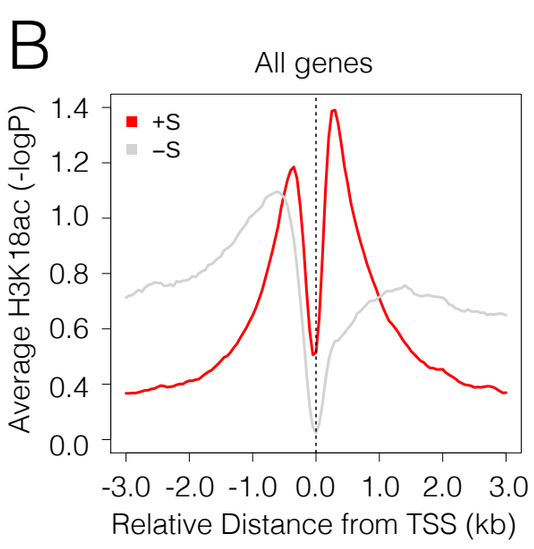

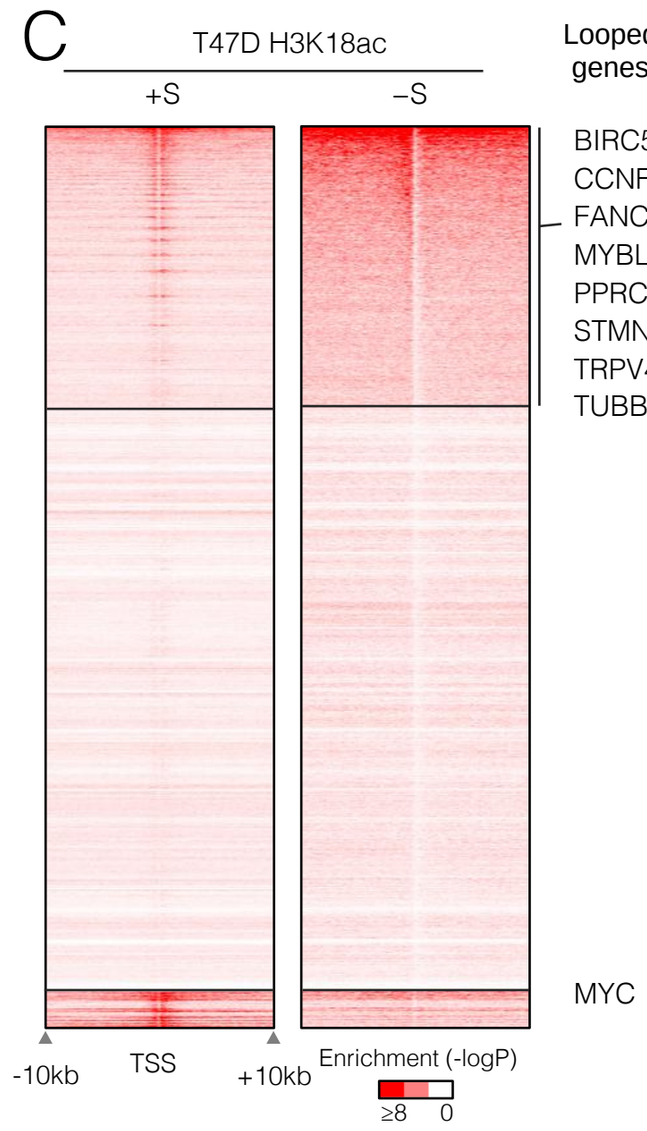

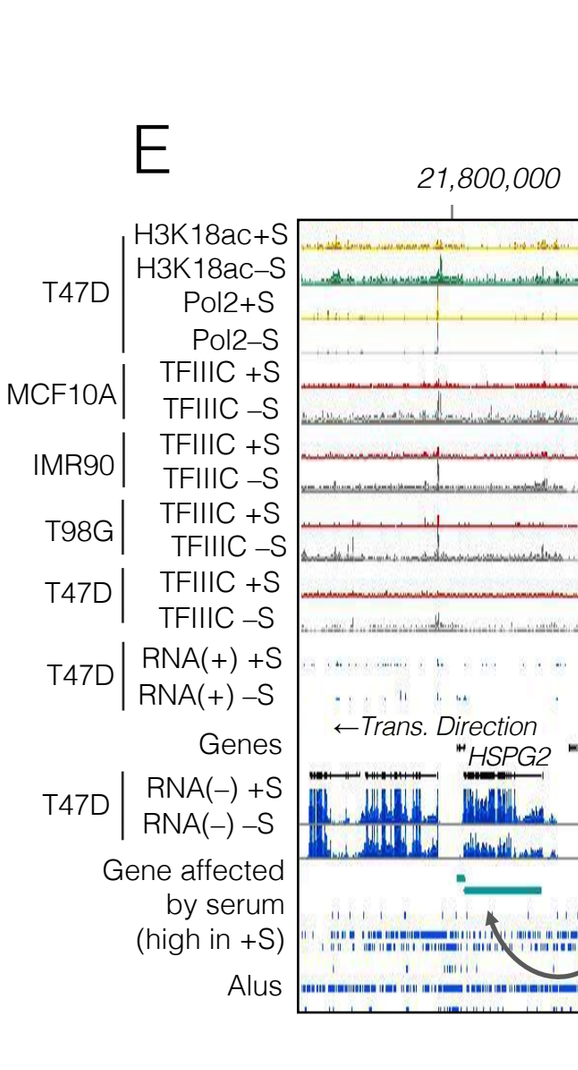

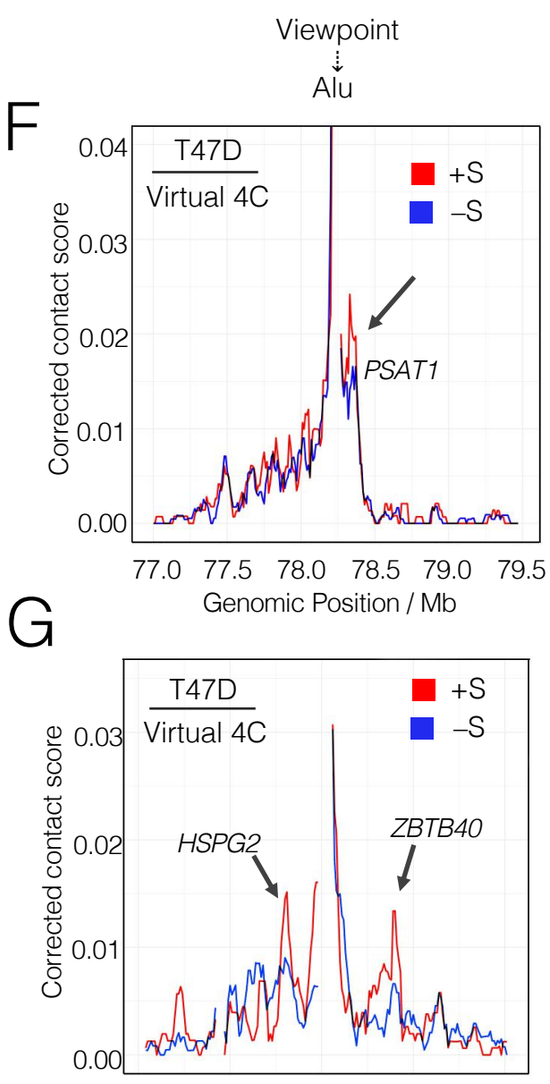

Supp. Figure 7

A

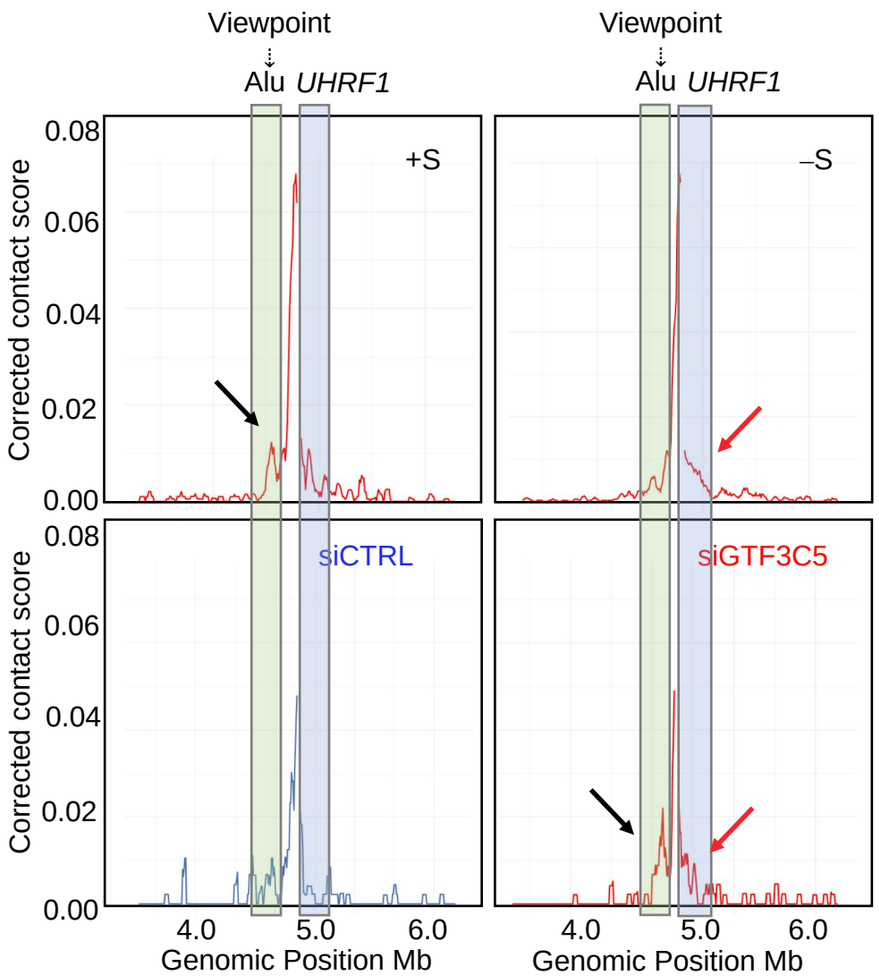

B

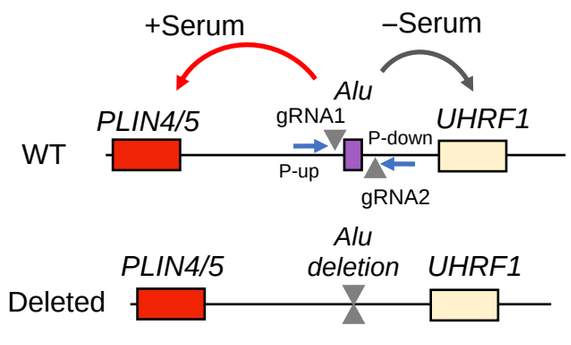

C

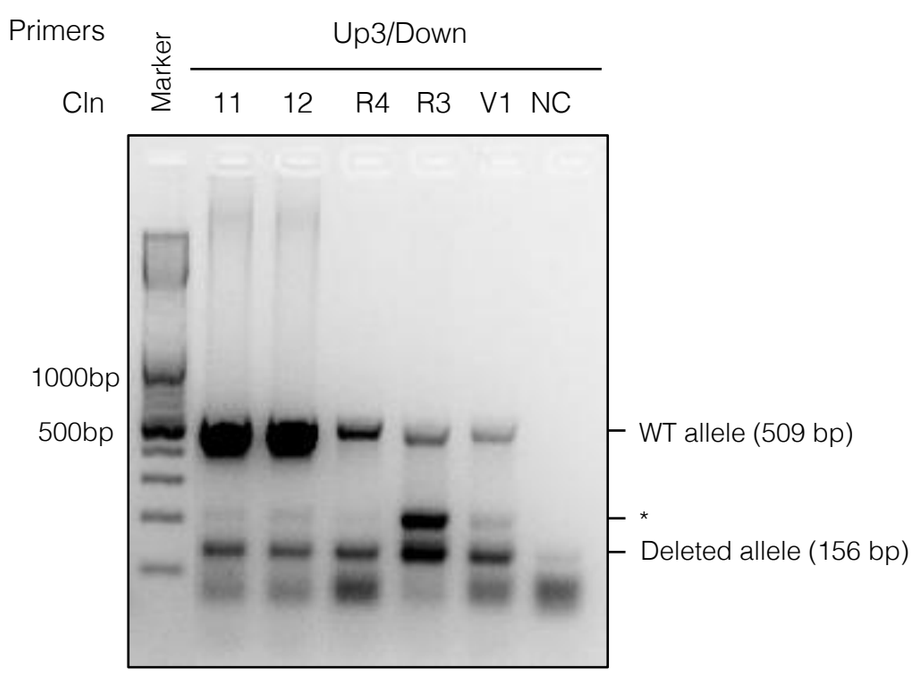

D

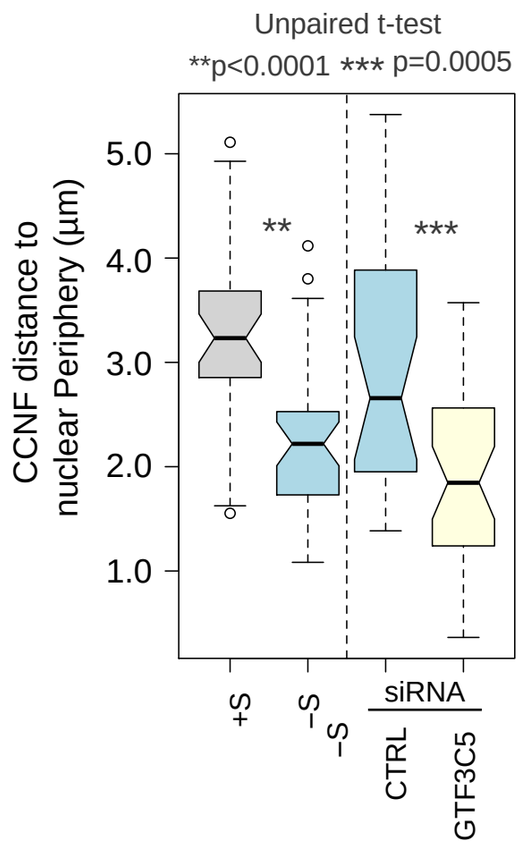

E

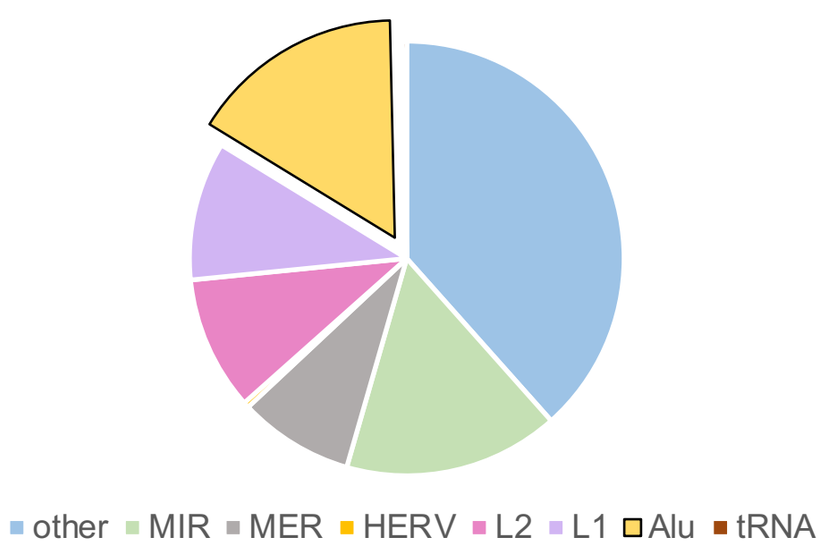

G

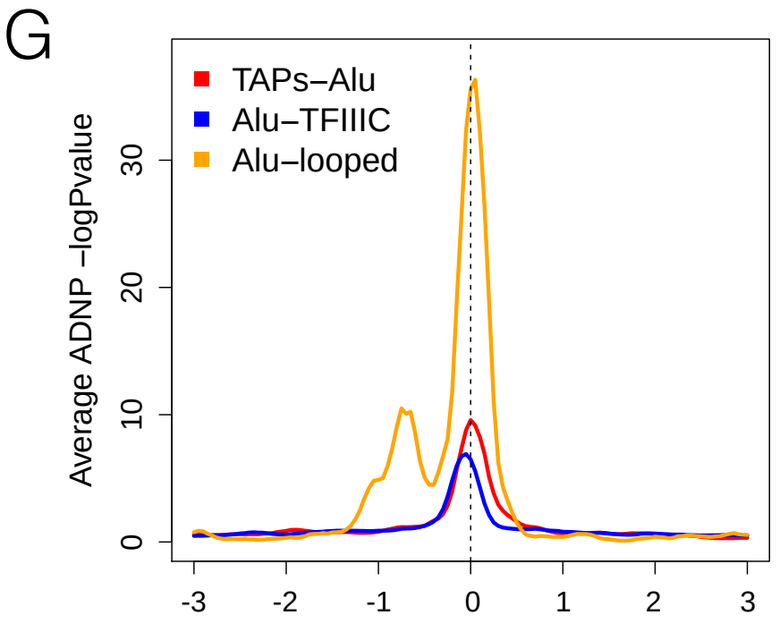

G

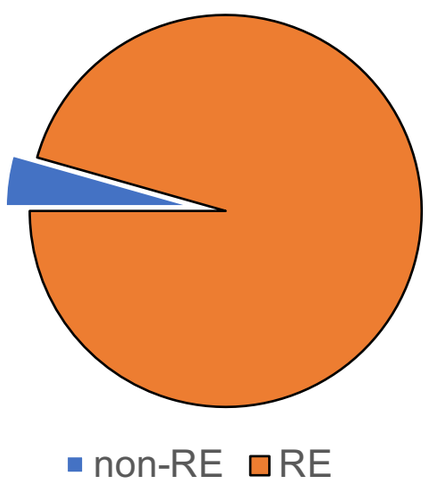

H

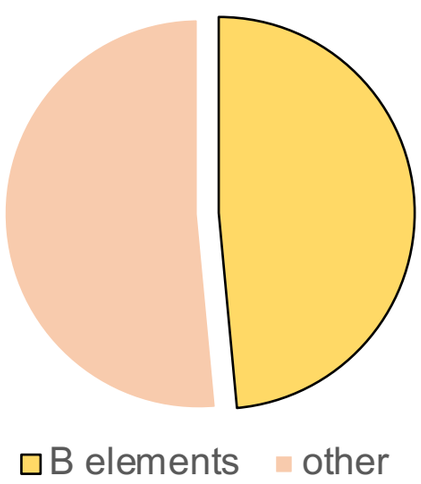

I

J

K